Dissertation zur Erlangung des Doktorgrades
der Fakultät für Chemie und Pharmazie
der Ludwig-Maximilians-Universität München

Characterization of *in vivo* chemoresistant human hepatocellular carcinoma cells with transendothelial differentiation capacities

von

Christian Frank Marfels

aus München

2015

Erklärung

Diese Dissertation wurde im Sinne von § 7 der Promotionsordnung vom 28. November 2011 von Herrn Prof. Dr. Ernst Wagner betreut.

Eidesstattliche Versicherung

Diese Dissertation wurde eigenständig und ohne unerlaubte Hilfe erarbeitet.

München, den 21. 01. 2015

.....
(Unterschrift des Autors)

Dissertation eingereicht am:	27.01.2015
1. Gutachterin / 1. Gutachter:	Prof. Dr. Ernst Wagner
2. Gutachterin / 2. Gutachter:	Prof. Dr. Stefan Zahler
Mündliche Prüfung am:	19.03.2015

Meiner Familie

Table of Contents

1 INTRODUCTION

1.1 Hepatocellular carcinoma

Hepatocellular carcinoma (HCC) is the fifth most frequent malignancy worldwide [1]. Moreover, its incidence increases due to hepatitis B and C viral infections, especially in countries where those viral infections are endemic such as China [2]. In countries with a high immunization rate against hepatitis B, cirrhosis is the main risk factor of hepatocellular carcinoma, mostly induced by alcohol abuse. Further risk factors are hemochromatosis, diabetis mellitus type II, and environmental toxins like Aflatoxin. The various factors and the often poor prognosis of HCC bring this disease into the focus of several treatment studies. Compared to other solid tumors, HCC is characterized by high levels of vascularization. The status of angiogenesis correlates with cancer progression and prognosis. Therefore, antiangiogenic strategies are suggested for treatment of HCC [3] due to survival advantages, as revealed in recent studies[4, 5].

1.2 Angiogenesis as a key player in tumor development

As angiogenesis performs a crucial and critical role in the development of many solid cancers [6-10], it's worthwhile to take a look at this phenomenon and its mechanism. Solid tumors are not vascularized as long as they are smaller then 2-3 cubic millimeters [11], because cells get oxygen and nutrients by diffusion comparable with small organisms like Drosophila melanogaster [12]. The angiogenic switch is a prerequisite for further tumor development and growth. The mechanism taking place between angiogenic switch and sprouting of new vessels into the hypoxic tumor tissue have been extensively reviewed in recent publications [12, 13]. The process of angiogenesis starts with the insufficient supply with oxygen in the cells, which are located around the core area of the solid tumor. Hypoxia inducible factor 1α (HIF-1α) switches on a complex signalling cascade [12]. The proangiogenic vascular endothelial growth factor (VEGF) family [14, 15] triggers the sprouting of an endothelial cell, the so called tip cell [16]. In the following sprouting process further signalling molecules, like neuropilins, Notch, phosphatidylinositol-

glycan biosynthesis class F protein (PIGF), and fibroblast growth factor (FGF), play an important role: they ensure the leading position of the tip cell and assure the directed growth of so called stalk cells [16]. Finally, VE-cadherin (vascular endothelial), CD34, VEGF, and hedgehog establish the lumen of the new vessel.
Functional blood vessels provide the basis of tissue homeostasis and growth with the supply of oxygen and nutrients and the elimination of metabolic degradation products [12]. Furthermore, the neovascularization improves the state of uncontrolled proliferation characteristic of tumor cells and is also thought to be an excellent indicator of its metastatic potential [17, 18]. Based on this knowledge, antiangiogenic therapies were introduced into clinic. The idea that blockage of angiogenesis could be a target in cancer therapy was postulated by Judah Folkman in 1971 [19]. Since then, many antiangiogenic drugs like antibodies against VEGF or its receptors and tyrosin kinase inhibitors were successfully used in cancer treatment against various solid tumors. For example: The monoclonal antibody against VEGF Bevacizumab was approved in combination with other chemotherapy for the treatment of metastatic colorectal cancer [20], non-small-cell lung cancer [21], metastatic renal cell carcinoma [22, 23], and metastatic breast cancer [24]. In addition, well-known cytotoxic drugs like cyclophosphamide (CPA) showed antiangiogenic capacities and were examined in different studies on their impact on angiogenesis [25, 26].

1.3 Cyclophosphamide – Pharmacology and medical uses

Cyclophosphamide is a well known cytostatic drug which is used in many therapeutic regimes against a bright range of tumors. As the oral application leads to bioavailability of more than 75% and also an intravenous (*i.v.*) application is possible, cyclophosphamide captured the market since its launch 1958. It is now state of the art in combination therapies against breast cancer, non Hodgkin lymphoma, acute lymphatic leukemia, and other sarcomas and blastomas. As a maximum tolerated dose (MTD) chemotherapy cyclophosphamide is used with 600 - 1000 mg/m² body surface area for intravenous application and depends on the kind of diagnosed tumor [27]. Uneffected by the way of application cyclophosphamide as a prodrug needs to be activated by the cytochrome P450 enzymes in the liver.

A member of the cytochrome P450, family 2, subfamily B (CYP2B) enzymes hydroxylates cyclophosphamide to 4-hydroxyphosphamide. This and its tautomer aldophosphamide are the transport-form and they diffuse into the tumor-cells. There, the last activation step takes place and aldophosphamide is decomposed into two compounds, acrolein and the cytotoxic phosphoramide mustard [28]. This active phosphoramide mustard alkylates irreversibly DNA and leads thereby to apoptosis [29].

1.4 Metronomic schedule of cyclophosphamide

The use of CPA in a preclinical antiangiogenic, metronomic regimen revealed encouraging results in terms of tumor growth suppression and survival in an *in vivo* rat model of hepatocellular carcinoma [30]. The metronomic treatment regimen is characterized by significantly reduced side effects, compared to conventional MTD chemotherapy administration and by anti-tumor activity in respect to its antiangiogenic properties. Preferentially, the metronomic treatment regimens target genetic stable tumor vessel endothelial cells and thus, the development of resistance against the therapy should be avoided [31, 32]. However, several studies point towards the induction of *in vivo* chemoresistance mechanisms that let tumors escape from metronomic CPA therapy [33-35].

1.5 Resistance during chemotherapeutic treatments

Many different mechanisms against chemotherapeutic agents are well known because of their efficiency in overcoming cancer therapies. The focus is on possible escape tools of cancer cell during CPA treatment (Figure 1), as CPA was used for several experiments in this thesis. In case of CPA, a diminished uptake of the metabolites 4-hydroxycyclophosphamide and aldophosphamide is one of the mechanisms. Additionally, a higher efflux of these two intermediates by unspecific pumps makes the therapy inefficiently. Often detoxicating enzymes are upregulated and metabolize the drug or his intermediates to inefficient, non-toxic agents. In all three cases a lower intracellular dose leads to a lower efficiency against the mutated cell. Further escape mechanisms are modifications at the effector points. As CPA is

an alkylating agent, faster repairing of DNA damages saves the cell survival. Moreover, arresting of important transmitters or mutations of these transmitters helps cancer cells to overcome chemotherapy, because thereby apoptosis is avoided [36].

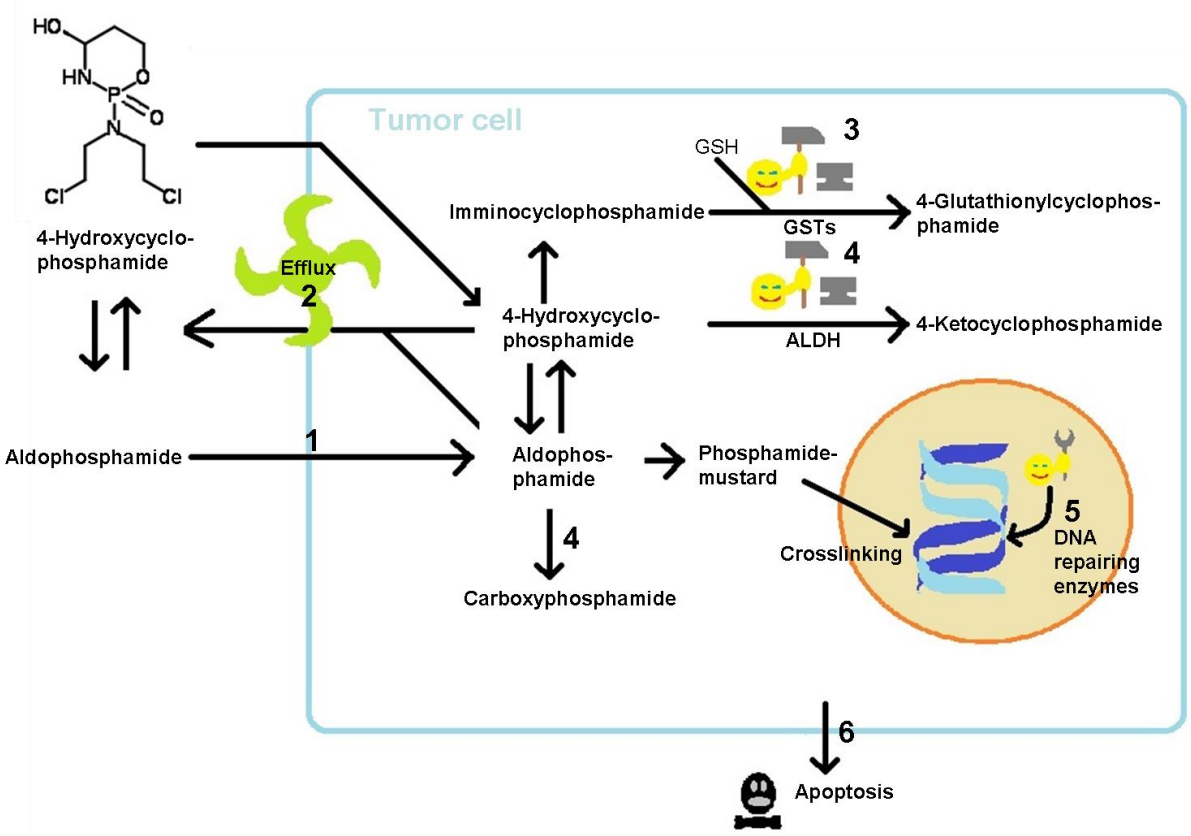

Figure 1 Possible escape mechanisms with its tools during CPA therapy. Diminished uptake (1), a higher number of efflux pumps on the cell surface (2), an upregulated detoxification by enzymes (3+4), and more DNA repairing enzymes (5) lead to a diminished effectiveness of CPA. Interruption of the apoptosis pathway is (6)

1.6 An *in vivo* chemoresistance HCC xenograft model

A novel *in vivo* chemoresistance HCC xenograft model was developed by Dr. Michael Günther in his PhD thesis (LMU Munich, 2007). Subcutaneous human hepatocellular carcinoma HUH-7 tumors were established in severe combined immunodeficiency (SCID) mice by injection of $5x10^6$ HUH-7 cells into the loin area of the animals. The untreated control group showed the aggressive manner of these tumors with a tumor volume doubling time of 2.5 days. With the metronomic scheduled CPA treatment of 75 mg/kg body weight every six days, Dr. Günther could

reach a growth delay and the tumor size of treated mice was constant up to day 75 after implantation. Afterwards, HUH-7-tumors in treated animals showed a volume doubling time of 3.5 days despite ongoing treatment and therefore, a resistance against therapy [37].

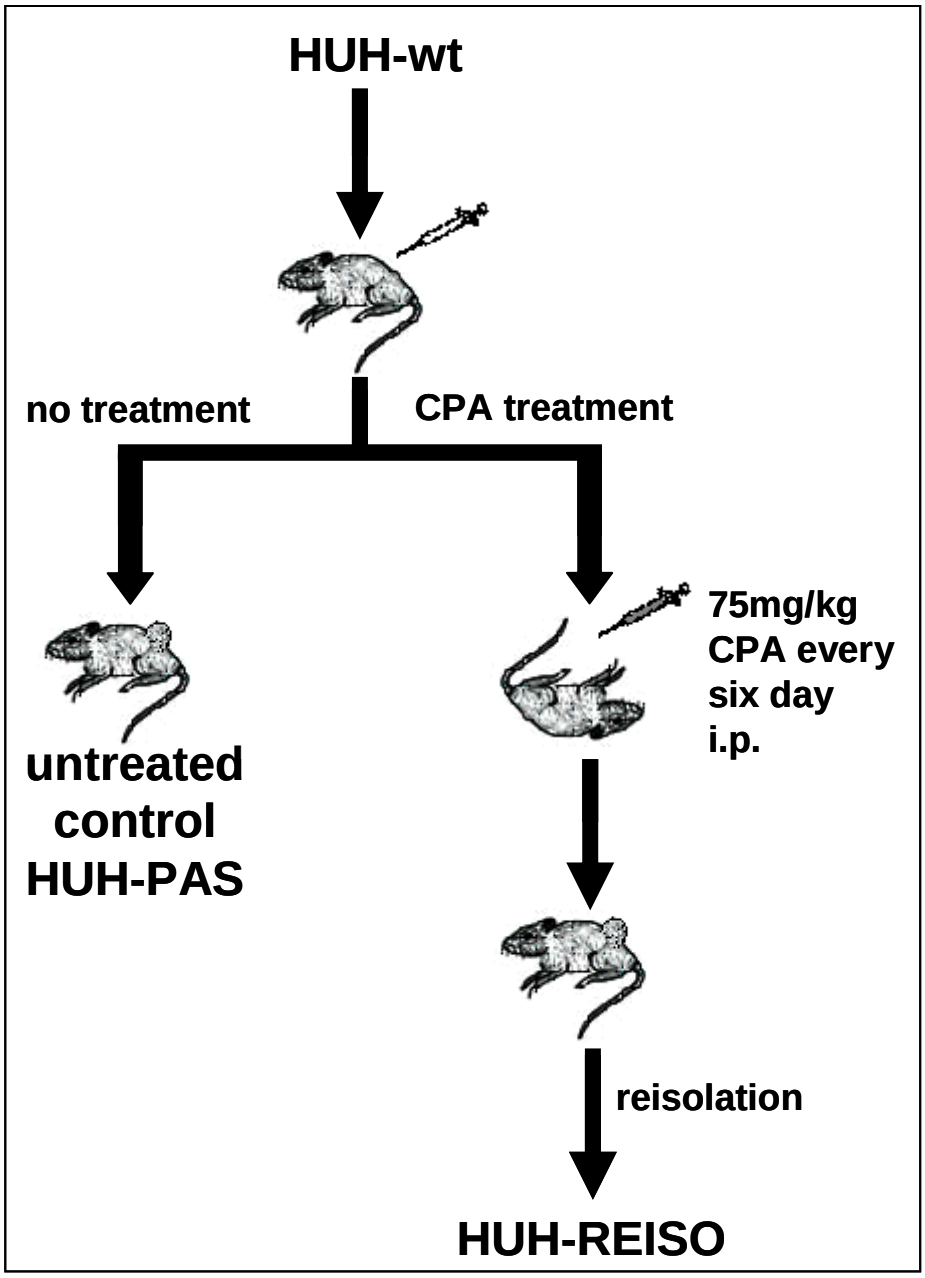

Figure 2: The human hepatocellular xenograft mouse model. Subcutaneous human HUH-7 tumours were established in SCID mice by injection of 5×10^6 HUH-7 cells into the flanks of animals (n=6). CPA treatment was started on day 12 after tumour implantation with 75 mg/kg CPA every six days. Metronomic scheduled CPA treatment resulted in significant tumour growth delay [37].

1.7 Aims of the thesis

In the current thesis, changes in transcription factors, controlling plasticity and stemness of tumor cells in an *in vivo* chemoresistance HCC xenograft mouse model should be investigated. The main objective was to discover targets for the therapeutic and also the diagnostic medicine in this chemoresistance model. On the one side, those should offer the correct diagnosis at an earlier time-point and on the other side, new options in therapy to overcome or even prevent resistance. Of course, many steps lie between the first identification and the successful therapy, but the origin of the problem has to be known for being able to solve the problem.

Resistant HCC xenografts were generated by metronomically scheduled CPA treatment in SCID mice, resulting in resistant tumor outgrowth after an initial chemoresponsive phase of 10 weeks. The histological analysis of the *in vivo* generated tumor tissue revealed significant changes in tissue organization and blood flow. In cell culture, cultivated cells of those *in vivo* generated cell lines lacked chemoresistance. But re-xenografted tumors from HUH-REISO cell culture manifested immediate chemoresistance, lacking an initial response phase.

Therefore, a more detailed view on the intracellular fingerprint of these cells should be generated: In order to detect gene expression associated with the chemoresistance and its development, expression levels of different markers had to be determined. Notch homolog 1, translocation-associated (Drosophila) (Notch-1), downstream hairy and enhancer of split-1 (HES-1), and neurogenic locus notch homolog protein 3 **(**Notch-3) are often described to have an important part in angiogenesis and were therefore part of the planned investigations. Moreover, the thesis should focus on the popular markers of stemness thymocyte antigen 1 (Thy-1), octamer binding transcription factor 4 (Oct-4), sex determining region Y box 2 (Sox-2) and Nanog. In *in vivo* passaged control tumor xenografts and in their resistant tumor counterparts with and without therapeutic pressure they should be investigated. Furthermore, several aspects of cell differentiation should be tracked in specialized *in vitro* models, mimicking features of environmental properties of solid tumors.

2 MATERIALS AND METHODS

2.1 Cell culture

Cell culture media, antibiotics, fetal bovine serum (FBS) and trypsin/EDTA solution were purchased from Invitrogen GmbH (Karlsruhe, Germany). Human hepatoma cells (HUH-7) (JCRB0403) were cultured in a mixture of Ham's-F12 and Dulbecco's modified Eagle's medium (DMEM) in a ratio of 1:1 supplemented with 10% FBS. Cells were grown at 37° C in 5% CO_2 in a humidified atmosphere. HUH-7 cells were cultured without antibiotics for at least 3 – 4 passages before tumor cell implantation and were harvested just as reaching approx. 70% confluency.

2.2 *In vivo* animal models

Male SCID mice (CB17/Icr-PrkdcSCID/Crl) (8–10 weeks) were housed in individually vented cages under specific pathogen free conditions with a 12 hours day/night cycle and with food and water *ad libitum*. HUH-7 cells were cultured as described above. The number of 10^6 HUH-7 cells in 100 µl phosphate buffered saline (PBS) was injected subcutaneously with a 25 G needle (Braun, Melsungen, Germany) into the flank of SCID mice. The animals were checked regularly for tumor progression. The moment that tumor volume reached the size of at least 10 mm^3, tumor progression was monitored using a digital measuring slide (Digi-Met, Preisser, Gammertingen). Each measurement consisted of three diameters, length (a), width (b), and height (c). Tumor volume was calculated by the formula $a \times b \times c \times \pi / 6$ (with a, b and c indicating the three diameters and $\pi / 6$ as correction factor for tumor shape). Tumor volume doubling time (TVDT) was calculated with $TVDT = \ln 2 \times (t2-t1) / \ln[V(t2)/V(t1)]$. All animal experiments were performed with 6 animals per group. All animal procedures were approved and controlled by animal experiments ethical committee of Regierung von Oberbayern, District Government of Upper Bavaria, Germany and carried out according to the guidelines of the German law of protection of animal life.

2.3 Isolation of tumor cells

For isolation of tumor cells, mice were sacrificed at the first therapy endpoint (see Figure 3 and Table 1) with CO_2. Skin was cleaned and sanitized with isopropanol (70% in water v/v), followed by drying under sterile conditions. Tumors were collected and immediately immerged in a 1:1 mixture of Ham's-F12 and Dulbecco's modified Eagle's medium (DMEM), supplemented with 10% FBS and 2% penicillin/streptomycin (Biochrom, Berlin, Germany). Tumor tissue was reduced to small sections under sterile conditions. Pieces were chosen randomly from all areas of the tumor. This procedure was repeated until the tumor tissue was homogenized. The obtained homogenized cell suspension was diluted with fresh penicillin/streptomycin containing Ham's-F12 and DMEM 1:1. The tumor cell containing suspension was transferred to tissue 6-well-plates (TPP, Trasadingen, Switzerland) and incubated under standard conditions (37 °C, 5% CO_2) in a humidified atmosphere for 2 - 3 days. Just as cells attached to the bottom of the plate, medium was replaced every second day, until cells reached a confluence of about 70%. Obtained cell lines (HUH-PAS, HUH-REISO) were defined in table 1. Reimplantation studies were performed by injection of 10^6 HUH-7 tumor cells at a passage number below 10.

Abbreviation	Origin of cells
HUH-wt	parental human hepatoma cell line (JCRB0403)
HUH-PAS	reisolated HUH-7 cells from HUH-wt tumors (non resistant)
HUH-REISO	reisolated HUH-7 cells from HUH-wt tumors after therapy (resistant)

Table 1 Abbreviations of cell lines and their origin

2.4 Transmitted light microscopy of cell culture

Transmission light microscopy of living cells growing as a monolayer in a 75 cm^3 cell culture flask (TPP, Switzerland) was performed using an Axiovert 200 microscope (Carl Zeiss, Jena, Germany) with an Infinity 2 camera and Infinity capture software (both: Lumenera corporation, Ottawa, Canada).

2.5 Chemotherapy

Cyclophosphamide (CPA) (Sigma, Taufkirchen, Germany) was solved in PBS (10 mg/ml) and applied intraperitoneally (i.p.). 75 mg/kg CPA solution was administered with a 25 G needle (Braun, Melsungen, Germany). The application of the CPA solution was carried out every 6 days. A single dose of each application was based on animal body weight. Toleration of CPA treatment was monitored by regular measurement of body weight. The vehicle group (PBS) and the drug treatment group (CPA dissolved in PBS) were housed separately.

2.6 Hematoxylin and eosin stain (HE stain) of tumors

Cryosections were fixed with 4% paraformaldehyde and stained with haematoxylin (Sigma, St. Louis, USA) for 30 minutes. After washing with PBS and distilled water (aqua dest.), sections were incubated with eosin (1:100 in aqua dest.) (Sigma, St. Louis, USA) for 4 minutes. Afterwards, sections were washed with aqua dest., embedded with PBS and analyzed by transmission light microscopy at the Axiovert 200 microscope (Zeiss, Jena, Germany).

2.7 Immunohistochemistry

For immunohistochemistry, tumors were embedded in tissue freezing medium (Jung, Nussloch, Germany). They were cut into sections of 5 - 10 µm thickness with a cryomicrotome (Leica CM 3050s, Wetzlar, Germany) at − 20 °C. Sections were transferred to a microscope slide, tissue freezing medium was removed and tissue was fixed with 4% paraformaldehyde (in PBS). Afterwards, sections were rehydrated and washed with blocking solution (PBS containing 5% FBS) prior to antibody incubation. Antibodies, which were used for staining are listed in Table 2. All primary antibodies were diluted 1:200 in blocking solution. After incubation for 12 hours at 4 °C in humidified atmosphere, sections were washed repeatedly with blocking solution followed by secondary antibody staining. Secondary antibodies were diluted 1:400 in blocking solution and sections were incubated for 2 hours at room temperature in humidified atmosphere. Sections were washed with blocking solution

repeatedly, before fluorescence analysis at the Axiovert 200 microscope (Zeiss, Jena, Germany) using appropriate filter sets.

Antigen	Primary Antibody	Secondary Antibody
human CD31 (PECAM-1)	mouse-anti-hum CD31 (Invitrogen, Carlsbad , USA)	goat-anti-mouse-Cy5 (Jackson, West Grove, USA)
mouse CD31 (PECAM-1)	rat-anti-mouse CD31 (BD, Franklin Lakes, USA)	goat-anti-rat-Alexa 488 (Invitrogen, Carlsbad , USA)
Laminin	rabbit-anti-laminin (Novus, Littleton, USA)	goat-anti-rabbit-Texas Red (Vector, Burlingame, USA)
negative Control hCD31	mouse IgG1 (Dako,Glostrup, Denmark)	goat-anti-mouse-Cy5 (Jackson, West Grove, USA)
negative Control mCD31		goat-anti-rat-Alexa 488 (Invitrogen, Carlsbad , USA)
negative Control Laminin		goat-anti-rabbit-Texas Red (Vector, Burlingame, USA)

Table 2 Antibodies used for immunohistochemistry.

2.8 Flow cytometry

2.8.1 Sample preparation *in vitro*

Cells, grown at 37 °C in 5% CO_2, were harvested, just as reaching approximately 70% confluency. After counting, 300,000 cells were subjected to each antibody staining.

2.8.2 Immunostaining for FACS analysis

Cells were washed twice with 5% fetal bovine serum FBS in PBS (FACS-buffer) prior to imunnostaining. Primary antibodies were dissolved 1:200 in FACS-buffer and cells were incubated with 200 µl of this dilution for 2 hours on ice. After two washing steps with 1 ml FACS-buffer, cells were stained with 200 µl of a 1:400 dilution of secondary antibody in FACS-buffer for 1 hour on ice. To avoid cell clumping and a concentration gradient of antibody in solution, cell suspension was regularly shaken during incubation. After a further washing step, stained cells were subjected to FACS analysis. Used primary and secondary antibodies are listed in Table 3.

Antigen	Primary antibody	Secondary antibody
human EGF-receptor	mouse-anti-human-EGF antibody (Dako, Glostrup, Denmark)	AlexaFluor488 goat-anti-mouse-antibody (Invitrogen, Carlsbad,USA)
negative controll	mouse IgG1, negative control antibody (Dako, Glostrup, Denmark)	AlexaFluor488 goat-anti-mouse-antibody (Invitrogen,Carlsbad,USA)

Table 3 Antibodies used for *in vitro* control of new generated cell lines.

2.8.3 FACS analysis

FACS analysis was performed using a CYAN LX High Performance Flow Cytometer (DakoCytomation, Copenhagen, Denmark). After sample preparation, stained cells were filtered to dissolve aggregates and 1 µl of 4',6-diamidino-2-phenylindole (DAPI) solution (1 mg/ml) was added. The measurement was performed using appropriate filter sets and excitation wavelength. Cell debris and doublets were excluded by appropriate gates, using forward versus sideward scatter, respectively sideward scatter versus pulse width scatter. At least 10,000 to 50,000 gated cells were measured.

2.9 Agarose overlay method

Cells were seeded in 6-well plates 24 hours before addition of the agarose overlay. Culture medium was removed and replaced with 1 ml medium containing 0.6% (w/v) agarose (Invitrogen, Carlsbad, USA). The agarose-containing medium was obtained by stepwise dilution of complete medium with melted agarose (5% agarose in

medium without supplementations, w/v). Before applying the agarose-containing medium to the seeded cells, the medium was allowed to cool to 37° C. After solidification, 2 ml of complete culture medium without agarose was added to the cells.

2.10 Spheroid growth in agarose gel

To avoid cell growth in a two dimensional way, cells were seeded into an agarose gel. Therefore, cells were harvested as soon as reaching approx. 70% confluency. The gel was prepared by mixing low melting agarose from Cambrex BioScience (Rockland, USA) with medium in a percentage of 10% (w/v). After autoclaving, the gel was diluted with medium to 1.2%. Afterwards gel and single cell suspension were mixed and 5,000 cells in 1 ml of 0.6% gel were seeded in a 24 well plate (TPP, Trasadingen, Switzerland). Grown spheroids were counted after 42 days. Pictures were taken with an Infinity 2 camera and Infinity capture software (both: Lumenera corporation, Ottawa, Canada).

2.11 *In vitro* matrigel angiogenesis assay

Matrigel was purchased from BD (Franklin Lakes, USA). The coating procedure was done as described in the BD guidelines for thin gel layers. Matrigel was thawed over night at 4 °C. After short homogenization of the gel by pipetting with cooled tips, 10 µl of matrigel were added to each well of a µ-slide angiogenesis uncoated chamber (ibidi, München, Germany). The slide was incubated for 30 minutes at 37 °C and afterwards cells were seeded on the gel layer in an amount of 50,000 cells in 50 µl of cell culture medium per well. Cells were grown at 37 °C in 5% CO_2 in a humidified atmosphere and observed with an axiovert 200 microscope (Zeiss, Jena, Germany). Pictures were taken after 24 hours with an Infinity 2 camera and Infinity capture software (both: Lumenera corporation, Ottawa, Canada). Image analysis was performed with the analysis software from S.Core (Hoehenkirchen, Germany).

2.12 qRT-PCR

Marker gene analysis was done by quantitative polymerase chain reaction. Therefore, pairs of primer were designed with the universal probe library of Roche and purchased from Metabion (Martinsried, Germany). All pairs of primer, which were used for qRT-PCR, are listed in Table 4. Total RNA of *in vivo* and *in vitro* samples were purified by using two different methods. For the *in vitro* angiogenesis assay samples, 10^6 cells were seeded on a thin layer of matrigel (BD, Franklin Lakes, USA) in a six well plate. Total RNA of cells from one well was purified by phenol-chloroform extraction using peqGOLD TriFast kit (Peqlab, Erlangen, Germany). Preparation of *in vivo* RNA-Samples was done with a NucleoSpin RNA II kit (Macherey-Nagel, Düren, Germany) using 30 mg of tumor tissue. 5 µg of purified RNA were applied for cDNA production. For each qRT-PCR 25 ng cDNA were used for amplification and all samples were measured in duplicates. After an activation cycle with 90 °C for 10 minutes, 45 cycles were performed with a 10 seconds denaturation step at 95 °C, 30 seconds of annealing at 60 °C and polymerase extension for 1 second at 72 °C. The PCR runs were performed with Light Cycler 480 (Roche, Mannheim, Germany). For detection, the corresponding probe out of the universal probe library (Roche, Mannheim, Germany) was applied. Fold changes were calculated with the ΔΔCt-method. As glyceraldehyde 3-phosphate dehydrogenase (GAPDH) and beta-actin (Act-B) showed stable unregulated expression status over all tested tumor samples in initial experiments, GAPDH was used as reference gene for measurements of Oct-4, Thy-1, and aldehyd-dehydrogenase (ALDH-1) and Act-B for measurements of HES-1, Notch-3, Notch-1, Nanog, Sox-2, platelet endothelial cell adhesion molecule **(**PECAM-1/CD31), and Intercellular adhesion molecule 2 (ICAM-2). The ready to use Universal Probe Library (UPL) reference gene assays for GAPDH and ACT-B (Roche Diagnostics, Mannheim, Germany) were applied.

Target Gene	Primer	Melting Point [°C]	GC Content [%]	Probe-No.	Amplicon [nt]
PECAM-1	ggctgttgaatttcccacat	59	45	12	66
	tgctcttccaatttccaagg	60	45		
ICAM-2	caatgaattccaacgtcagc	59	45	75	70
	accaaagtgggttgcagtgt	60	50		
VEGFR2	gaacatttgggaaatctcttgc	59	41	18	66
	cggaagaacaatgtagtctttgc	60	43		
VE-cadherin	caacgagggcatcatcaag	60	53	42	78
	gtggcctcgacgatgaag	60	61		
vWF	ctgcacagtgacatggaggt	59	55	54	69
	catgttcccacccacgtaa	60	53		
HES-1	aaagatagctcgcggcatt	59	47	78	121
	gcacacttgggtctgtgct	59	58		
Oct-4	agcaaaacccggaggagt	59	56	35	114
	ccacatcggcctgtgtatatc	60	52		
Nanog	atgcctcacacggagactgt	60	55	69	66
	agggctgtcctgaataagca	59	50		
Sox-2	ttgctgcctctttaagactagga	59	43	35	75
	ctggggctcaaacttctctc	59	55		
Thy-1 (CD90)	aggacgagggcacctacac	60	63	22	107
	gccctcacacttgaccagtt	60	55		
Notch-1	cgcacaaggtgtcttccag	60	58	85	87
	aggatcagtggcgtcgtg	60	61		
ALDH-1	ccaaagacattgataaagccataa	59	33	82	77
	cacgccatagcaattcacc	60	53		
Notch-3	gccaagcggctaaaggta	59	56	30	65
	cactgacggcaatccaca	60	56		

Table 4 Pairs of primer used for qRT-PCR

2.13 *In vitro* CPA sensitivity

In vitro sensitivity was assayed by measuring the DNA content of a cell population composed of 25% of CPA activating X39 cells mixed with either HUH-wt, or HUH-REISO cells, followed by CPA treatment. Generation of cytochrome P450, family 2, subfamily b, polypeptide 1 (CYP2B1) transgene expressing X39 cells is described previously [38]. In total, 1,500 cells per well were plated in 48-well plates. Twenty-four hours after seeding, the culture medium was removed and replaced by either 200 µl

of fresh medium or by fresh cell culture medium containing CPA at the indicated concentrations. Treated cells and controls were incubated for 5 days in a humidified atmosphere containing 5% CO2 at 37 °C. DNA contents were assayed after Hoechst 33258 incorporation, as previously described [38]. Briefly, cells were lysed with Millipore water followed by a freeze–thaw cycle. Cell lysis buffer (1 mM Tris-EDTA, pH 7.4, 200 mM NaCl) containing 0.2 ng/ml Hoechst 33258 was applied to each well, followed by another freeze–thaw cycle. The DNA content was measured by quantifying fluorescence with a plate reader (Tecan, Grödig, Austria) equipped with filters for excitation at 360 nm and emission at 465 nm. Relative DNA content was calculated using the ratio of DNA content treated /DNA content untreated cell culture.

2.14 Statistical analysis

U-Test (Mann-Whitney) analysis was performed with WinStat for Exel to proof statistical significance in all cases. * stands for p≤0.05, ** for p≤0.01

2.15 Chemicals and reagents

Chemicals	**Supplier**
Agarose	Invitrogen (Carlsbad, USA)
Cyclophosphamide	Sigma (Taufkirchen, Germany)
DAPI	Sigma Aldrich (Germany)
DMEM	Invitrogen GmbH(Karlsruhe, Germany)
EDTA Solution	Invitrogen GmbH (Karlsruhe, Germany)
Eosin	Sigma (St. Louis, USA)
Fetal Bovine Serum	Invitrogen GmbH (Karlsruhe, Germany)
Ham’s F12	Biochrom (Berlin, Germany)
Haematoxilin	Sigma (St. Louis, USA)
Hoechst 33258	Sigma Aldrich (Germany)
Low Melting Agarose	Cambrex BioScience (Rockland, USA)
Matrigel	BD (Franklin Lakes, USA)
NucleoSpin RNA II Kit	Macherey-Nagel (Düren, Germany)

Paraformaldehyde	Sigma Aldrich (Germany)
Penicillin/Streptomycin	Biochrom (Berlin, Germany)
PeqGOLD TriFast Kit	Peqlab (Erlangen, Germany)
Tissue Freezing Medium	Jung (Nussloch, Germany)
Tris base	SIGMA-Aldrich (Steinheim, Germany)
Trypsin	Invitrogen GmbH (Karlsruhe, Germany)

.

3 RESULTS

3.1 HUH7 tumors under metronomic CPA therapy *in vivo*

Male and female SCID mice bearing subcutaneously implanted human HUH7 tumors were treated with metronomically scheduled CPA (75 mg/kg every 6 days). CPA treatment was started on day 12 after tumor cell implantation, just as tumors reached an average volume of 32 mm^3. Metronomically scheduled CPA treatment resulted in a significant tumor growth delay. The tumor volume of treated mice was constant at around 100 mm^3 up to day 75 after tumor cell implantation, whereas tumors in the control group exhibited a tumor volume doubling time of 2.5 days. Around day 75 after tumor cell implantation, tumor volume began to increase in the CPA treated group, with a tumor doubling time of 3.5 days, despite ongoing treatment (Figure 3). Metronomically scheduled CPA therapy was well tolerated, indicated by a constant animal body weight up to day 85 after tumor cell implantation. Further CPA treatment resulted in significant loss of body weight, observed in all CPA treated animals. Treatment was stopped and the mice were sacrificed as soon as the average body weight loss reached 20%. At this therapy endpoint, tumors were collected and subjected to macroscopical and histological analyses. Furthermore, tumor cells were extracted from viable tumor tissue for characterization and cell culture experiments. To establish appropriate control cells (HUH-PAS), HUH7 were grown in male and female SCID mice, without exposure to therapy. As soon as tumors reached about 300 to 400 mm^3, viable cells were extracted from the tumor tissue [37].

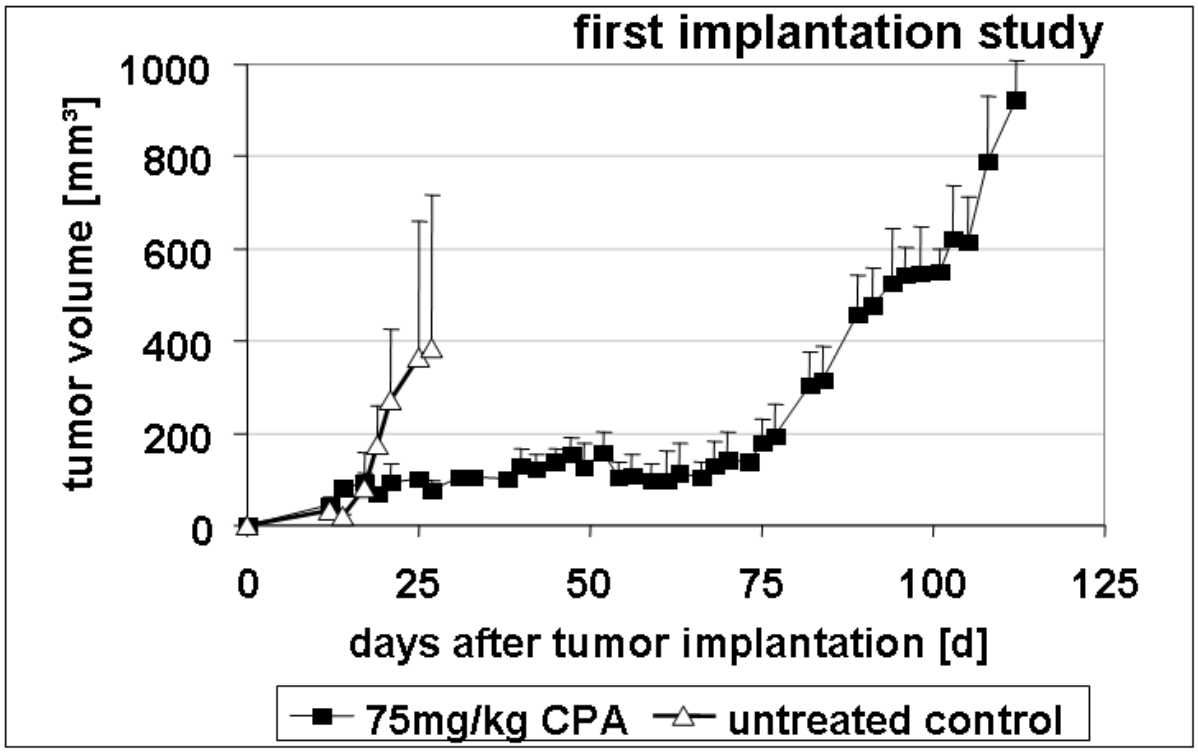

Figure 3: First implantation study. Subcutaneous human HUH-7 tumors were established in SCID mice by injection of 5×10^6 HUH-7 cells into the flanks of animals. CPA treatment was started on day 12 after tumor implantation with 75 mg/kg CPA every sixth days. Metronomically scheduled CPA treatment resulted in significant tumor growth delay. Tumor volume of treated mice was constant up to day 75 after tumor cell implantation, whereas tumors in the control group exhibited a tumor volume doubling time of 2.5 days. Around day 75 after tumor cell implantation, tumor volume began to increase in the CPA treated group despite ongoing treatment with a tumor doubling time of 3.5 days. Experiments performed by Michael Günther, PhD thesis LMU 2007

3.2 *In vitro* control of new generated cell lines

Reisolated cells (HUH-REISO and HUH-PAS) were analyzed for their human origin *in vitro* to exclude contamination by mouse cells. First, their morphology was checked by transmitted light microscopy and compared to the parental HUH-wt. All three cell lines grew in isles of small and polygonal cells and hence displayed typical morphology for epithelial cells (Figure 4 A-C). No cells with different morphology appeared in any cell line. Second, cells were identified by human epidermal growth factor-receptor (EGF-receptor) staining for their human origin. The following FACS

analysis showed that all cell lines were positive for hEGF-R and had therefore only human origin (Figure 4 D-F).

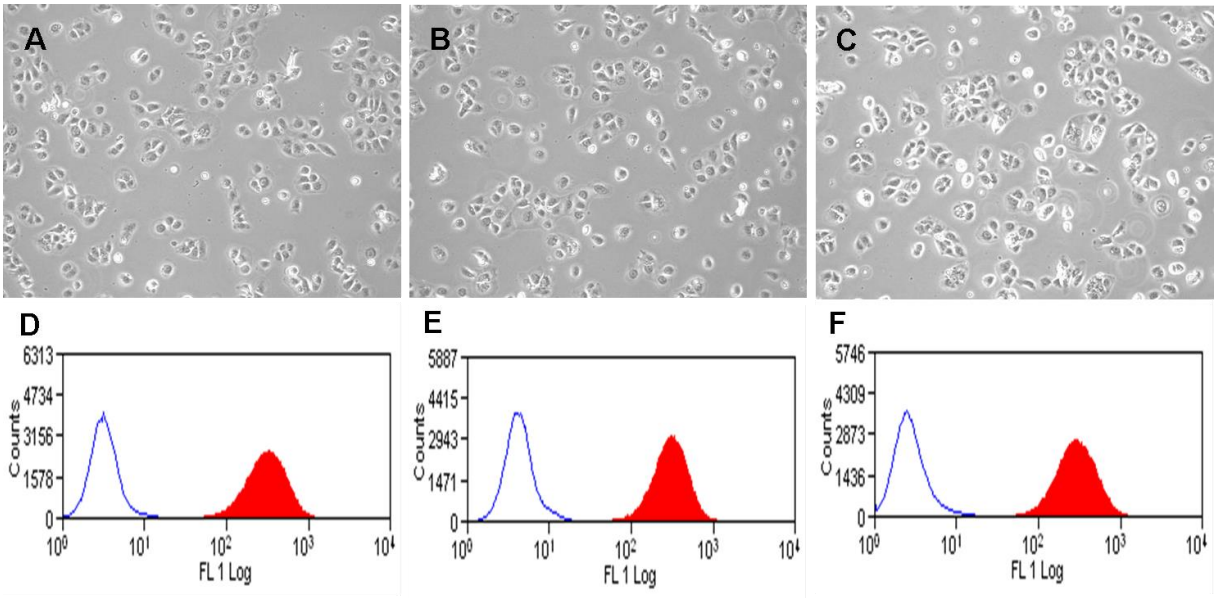

Figure 4: Microscopic pictures of cell cultures and FACS analysis for human origin of all HUH cell lines. HUH-wt (A), HUH-PAS (B) and HUH-REISO (C) showed no differences in morphology by transmitted light microscopy. In FACS analysis, cells showed human origin in the hEGF-receptor-staining : The whole population of HUH-wt (D), HUH-PAS (E) and HUH-REISO (F) shifted completely indicated by the red curve in comparison to the correspondent control antibody (white curve).

3.3 Influence of CPA therapy on tumor macroscopic appearance, tumor histology and functional blood flow

Tumors at the first therapy endpoint were macroscopically assessed. The tumor tissue appeared dark and bloody (HUH-REISO) (Figure 5 D), compared to the untreated control tumors (HUH-wt) (Figure 5 A). For further characterization and evaluation of changes induced by *in vivo* passaging and CPA treatment, histological and immunohistological analyses were performed. Therefore, cryosections were stained with hematoxylin/eosin and analyzed by transmitted light microscopy. Tissue structure in the original HUH7 xenografts (established from HUH-wt) was compact and homogeneous (Figure 5 B). In contrast, resistant tumors (HUH-REISO) exhibited an inhomogeneous, sponge-like structure with large cavities within the tumor tissue

(Figure 5 E). These cavities were identified as intratumoral pools of blood, due to the presence of erythrocytes. To verify this finding, *in vivo* tumor blood flow was visualized by systemically applied Hoechst 33258 dye as a tracer. Several cavities within the tumor tissue from resistant HUH-REISO tumors exhibited tracer fluorescence, indicating connection with the systemic blood supply (Figure 5 F). For comparison, functional blood supply analysis was performed also for the original xenografted HUH7 tumors (HUH-wt, Figure 5 C) and re-implanted, treated HUH-PAS tumors (Figure 6 A-C). These HUH-PAS control tumors showed a clear diminished functional blood flow [37].

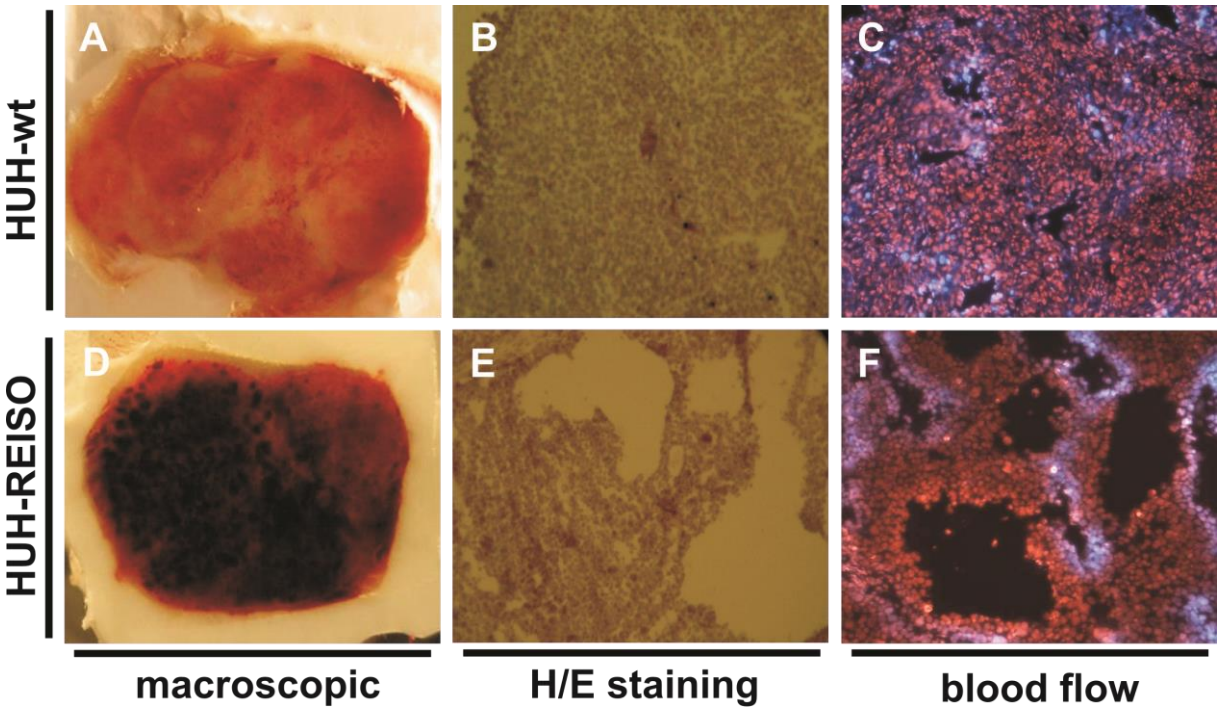

Figure 5: Macroscopic appearance, tumor histology and functional blood flow. (A-C) Untreated parental tumor (HUH-wt) and (D-E) CPA treated *in vivo* resistant tumor at treatment endpoint (HUH-REISO), all collected at day 25 after tumor cell implantation. Cryosections (8 µm) were fixed with 4% paraformaldehyde (PFA) and subjected to H/E staining: (B) shows untreated parental tumor (HUH-wt) and (E) *in vivo* resistant tumor at treatment endpoint (HUH-REISO). Functional blood flow was visualized by intravenous application of Hoechst 33258 dye (blue): (C) displays untreated parental tumor (HUH-wt) and (F) *in vivo* resistant tumor at treatment endpoint (HUH-REISO). Experiments performed by Michael Günther, PhD thesis LMU 2007

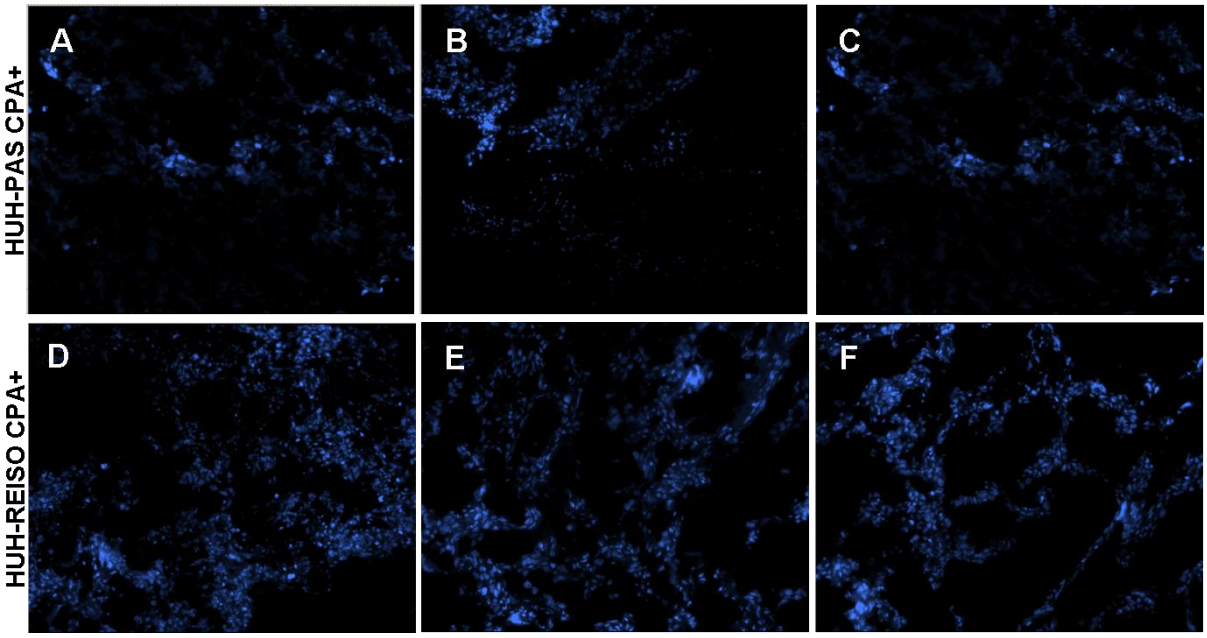

Figure 6: Hoechst-blood-flow comparison of HUH-REISO versus HUH-PAS after therapy. Intratumoral functional blood flow was visualized by intravenous application of Hoechst 33258 dye (blue). Cryosections (5 µm) of HUH-PAS control tumors after 2xCPA treatment (A-C) showed a clear diminished functional blood flow in comparison to treated HUH-REISO tumors (D-F). To ensure to have tumor material for analysis, the beginning of treatment was late for HUH-PAS tumors, when tumors reached an average volume of 254 mm^3.

3.4 Immunohistochemical analysis of vascular structures in xenografts

Immunohistochemical analysis of the vessel associated markers murine PECAM-1/CD31 and laminin showed an obvious shift from initial tumor vascularization (HUH-wt) (Figure 7 A), which is typical for HUH7 xenografts, to tumor tissue with a decreased murine vessel density (HUH-REISO) (Figure 7 B) at the therapy endpoint. Interestingly, functional blood flow, indicated by Hoechst tracer staining, was not closely correlated with immunohistochemically identified vessel structures (Figure 7 B) [37].

Regarding plasticity aspects, tumor tissue was stained for human, besides mouse, endothelial specific marker PECAM-1/CD31 (hPECAM-1 and mPECAM-1). Counter stain of cell nuclei with DAPI can be seen in Figure 7 C (HUH-wt), Figure 7 G (HUH-PAS) and Figure 7 K (HUH-REISO). Control stains revealed no hPECAM-1 signal for

the parental HUH7 xenografts (Figure 7 E and F), whereas mPECAM-1 (mCD31) positive cells showed a large network of vessel (Figure 7 D, highlighted with black arrows). Most interestingly, Figure 7 M and merged Figure 7 N showed hPECAM-1 (hCD31) positive structures (highlighted with white arrows) in re-implanted resistant xenografts (HUH-REISO) in close neighborhood to murine vascular structures (Figure 7L), indicating HCC plasticity towards the endothelial lineage. Control tumors of HUH-PAS, which were treated twice with CPA, showed rare positive signals for mPECAM-1 (Figure 7 H) and no positive signal for hPECAM-1 (Figure 7 I). Those HUH-PAS tumors had to be treated late, when they had reached an average volume of 254 mm^3. At an earlier starting point of therapy of these chemoresponsive cells there would not be enough tumor material left for reliable analysis (Figure 9).

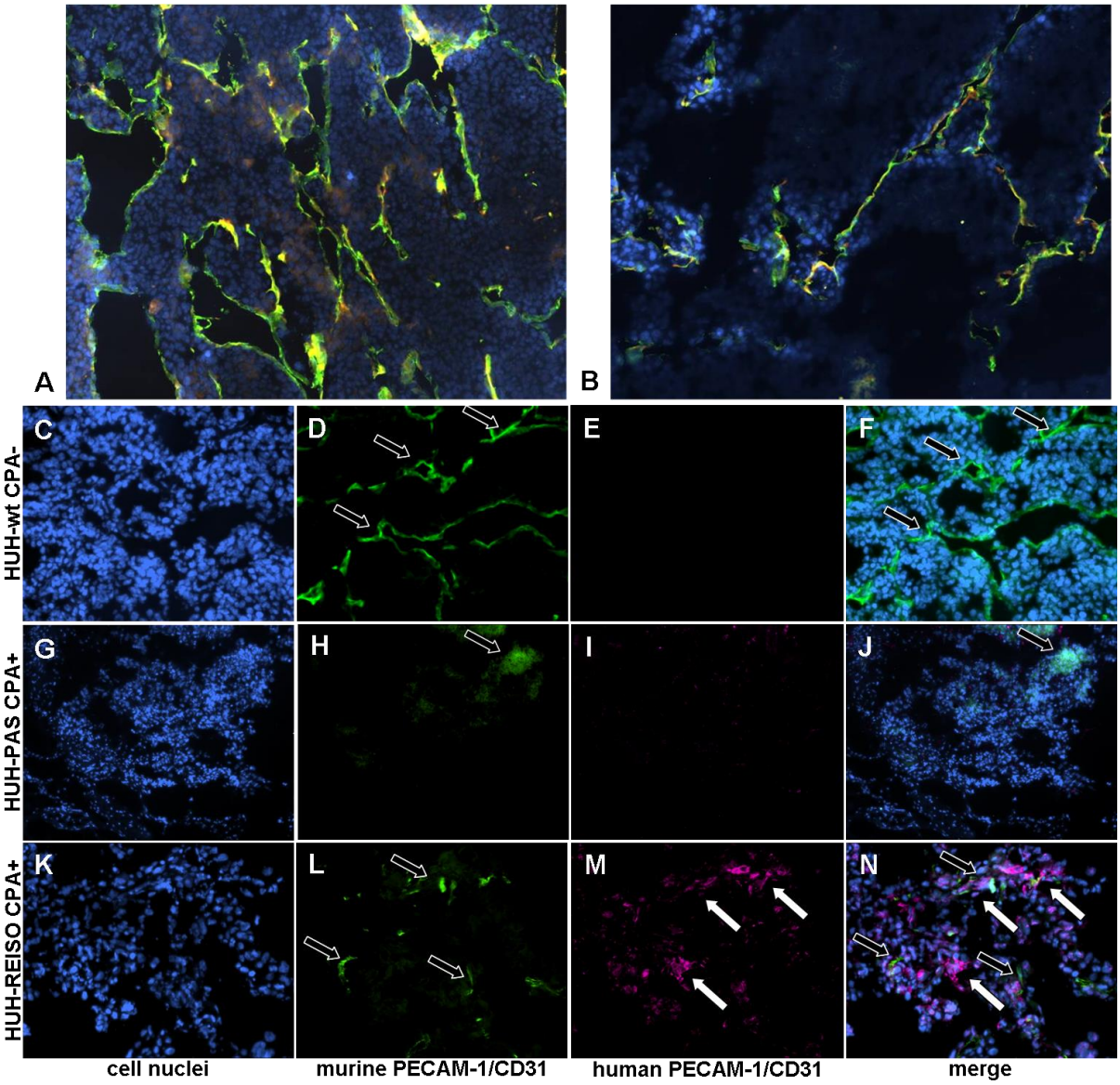

Figure 7: Immunohistochemical analysis for vascular markers in HUH-7 tumors. Cryosections (5 µm) of untreated control tumors (HUH-wt) (A) and CPA treated, chemoresistant tumors HUH-REISO (B) were fixed with 4% PFA and stained with antibodies for murine CD31/PECAM-1 (green) and laminin (yellow). Significant changes in the arrangement of laminin and CD31/PECAM-1 positive endothelial cells were detected in CPA treated tumors versus control tumors. Functional blood flow was visualized by intravenous application of Hoechst 33258 dye (blue). Experiments performed by Michael Günther, PhD thesis LMU 2007 (A+B)

Additional immunohistochemically stained cryosections of untreated HUH-wt (C-F) tumors, and HUH-PAS (G-J) or HUH-REISO (K-N) tumors after two times CPA treatment are shown. Staining for murine CD31/PECAM-1 (D/H/L, green, highlighted with black arrows) and human CD31/PECAM-1 (E/I/M, magenta, highlighted with white arrows) and cell nuclei were counterstained with DAPI (C/G/K). Additional to signals from murine CD31/PECAM-1,

significant human CD31/PECAM-1 expression was detected in (K-N, HUH-REISO) chemoresistant CPA treated tumors, whereas human CD31/PECAM-1 expression was not detected in (C-F, HUH-wt and G-J, HUH-PAS) control tumors.

3.5 No evidence of acquired resistance *in vitro*

Original HUH7 cells (HUH-wt) and HUH-REISO tumor cells were treated in an *in vitro* co-culture model together with X39 cells, expressing the CYP450 transgene to convert CPA in situ into activated CPA [38]. As shown in Figure 8, the *in vivo* resistant HUH-REISO as well as the HUH-wt cells showed CPA concentration-dependent decrease in cell proliferation, indicating no manifestation of resistance in the *in vitro* setting. Interestingly, the *in vivo* resistant HUH-REISO displayed an insignificantly higher chemosensitivity [37].

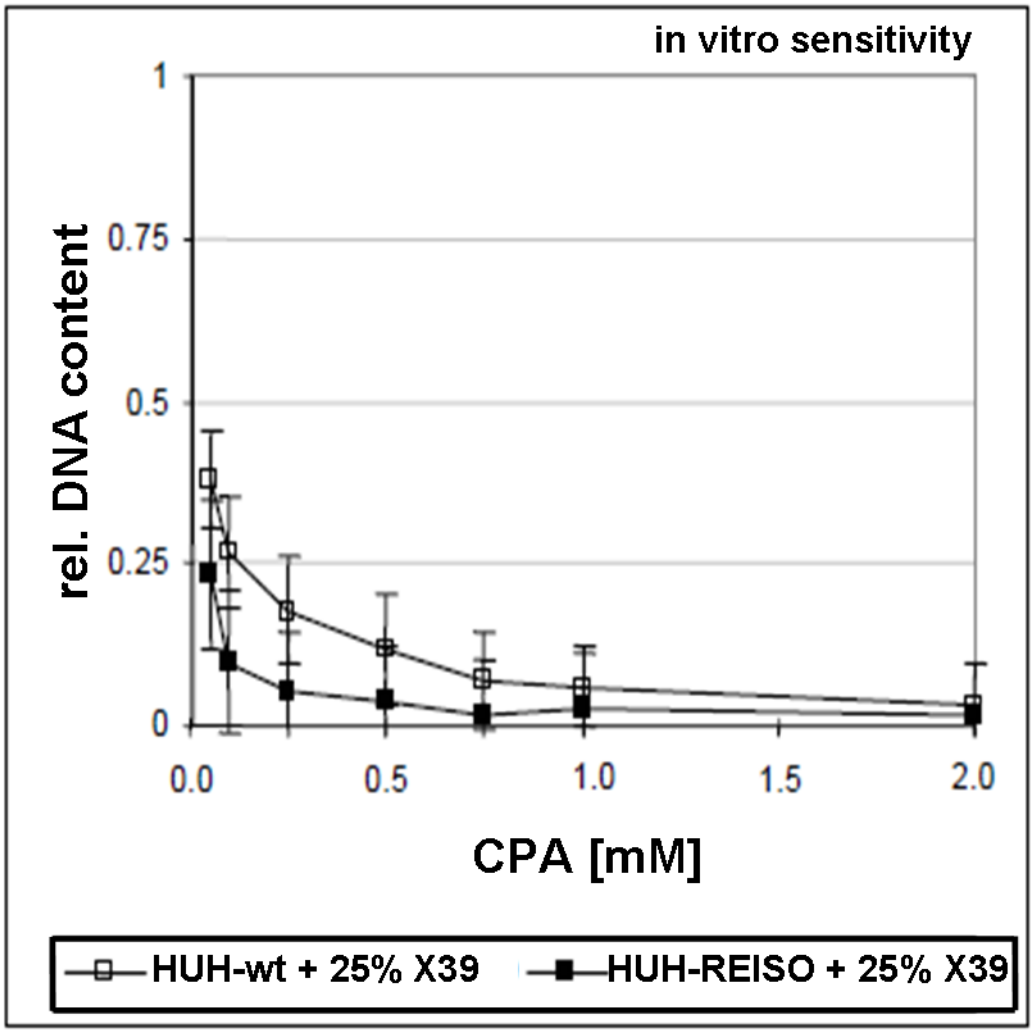

Figure 8: Sensitivity of parental HUH-wt and isolated HUH-REISO cells towards *in situ* activated CPA. Parental and isolated cells were treated with different concentrations of CPA for 3 days together with CPA activating cells X39. Proliferation was determined by measuring total DNA content per well. Control experiments were performed in the absence of CPA. Mean values ± SD of four measurements are shown. No significant differences were observed, nevertheless HUH-REISO cells showed higher sensitivity. Experiments performed by Michael Günther, PhD thesis LMU 2007

3.6 Resistance of re-implanted tumors towards metronomic CPA therapy *in vivo*

Re-isolated HUH-REISO tumor cells and re-isolated *in vivo* passaged (HUH-PAS) cells were implanted in the flank of SCID mice. On day 10 after tumor cell implantation, just as average tumor volume reached 14 mm^3, mice were subjected to

CPA treatment (75 mg/kg, every 6 days). Tumor volume and body weight were measured regularly during the treatment. No growth retardation effect was detectable for xenografts established from HUH-REISO cells, in contrast to blocked growth of xenografts established from *in vivo* passaged cells (HUH-PAS) (Figure 9). Resistant xenografts exhibited an average tumor volume doubling time of approximately 4.5 days. Metronomically scheduled CPA was again well tolerated, indicated by no significant loss in body weight.

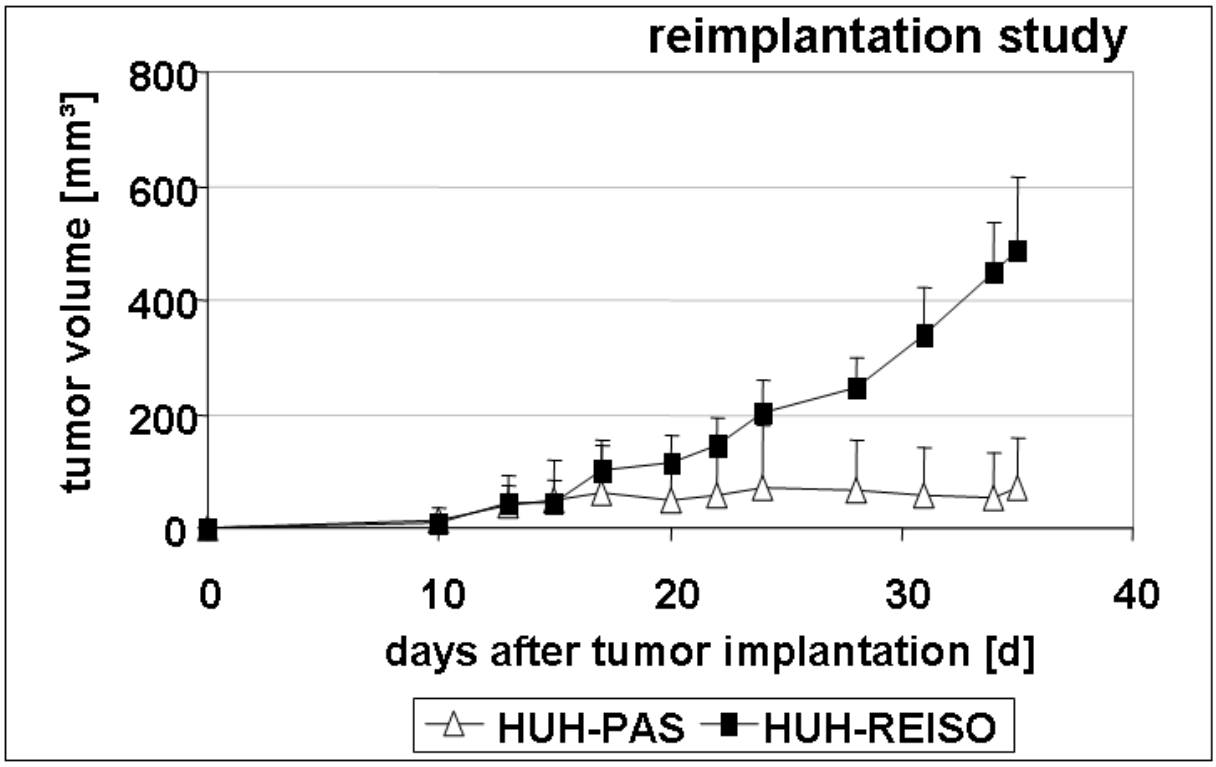

Figure 9: Re-implantation study. Cells isolated from resistant CPA treated tumors (HUH-REISO) were cultured *in vitro* and, after several passages, re-implanted in SCID mice (n=6) again, with CPA therapy (75 mg/kg every sixth days) starting at day 10 after cell implantation. A cell line established from *in vivo* passaged tumor cells (HUH-PAS) served as control. Tumors derived from HUH-REISO cells revealed a tumor volume doubling time (under therapy) of 4.5 days, whereas tumor growth in the control group was not evident within the observed time.

3.7 Regulation of ALDH-1 expression in response to CPA therapy *in vivo*

As *homo sapiens* aldehyde dehydrogenase 1 family member A1 (ALDH-1) is a known detoxification enzyme and inactivates CPA intermediates, expression levels were measured in HUH-REISO and in HUH-PAS during therapy. In absence of CPA pressure, only insignificant differences in expression levels were detectable in HUH-PAS and in HUH-REISO tumors (Figure 10). However, during therapy, expression levels of ALDH-1 increased in both xenograft types significantly after two treatments. In resistant tumors, ALDH-1 expression levels increased 2.5-fold after six treatments. With a p-value of 0.35, the ALDH-1 mRNA levels were not statistically different between HUH-PAS and HUH-REISO after the 2nd treatment (2xCPA).

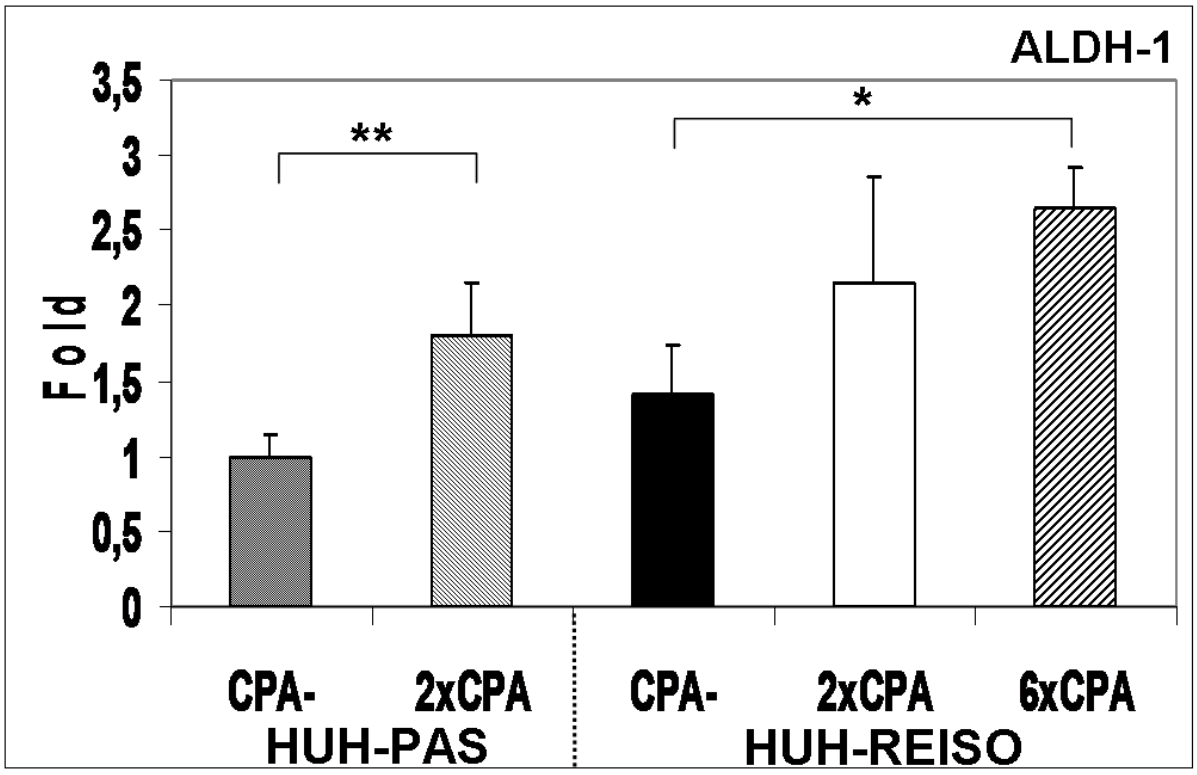

Figure 10: Aldehyde dehydrogenase I (ALDH-1) expression levels. Influence of CPA treatment on expression levels of ALDH-1 was determined in tumor tissue by qRT-PCR analysis after two treatments (HUH-PAS and HUH-REISO) and additional four treatments in the case of HUH-REISO (n=5). CPA therapy induced ALDH-1 expression in HUH-PAS (p=0.009) and in HUH-REISO (p=0.01) xenografts significantly. However, the ALDH-1 level was similar for passaged (HUH-PAS) and resistant (HUH-REISO) xenografts, independent of

therapy. Statistic evaluation was performed using the Wilcoxon-Mann-Whitney test. P< 0.05 was considered as significant and indicated by *, p< 0.01 was indicated by **.

3.8 Expression profiles of Thy-1, Oct-4, Sox-2 and Nanog *in vivo*

For characterization of stemness as a possible cause of tumor cell plasticity, the well established stemness markers Thy-1, Oct-4, Sox-2 and Nanog were analyzed, after total RNA extraction from tumor tissue. Expression analysis of untreated mice revealed that expression levels of Thy-1 (Figure 11 A), Oct-4 (Figure 11 B) and Nanog (Figure 11 D) were significantly increased in resistant tumors. In contrast to tumors, which were grown from HUH-PAS cells, Sox-2 (Figure 11 C) was not significantly increased in resistant tumors. In untreated resistant tumors, Thy-1 expression levels were about 100-fold (p=0.014) higher, Oct-4 expression levels were about 14-fold increased (p=0.027), Sox-2 expression levels were 5-fold (p=0.086) upregulated and expression levels for Nanog were detected to be increased about 7-fold (p=0.05), in comparison to tumors established from passaged tumor cells (Figure 11 A-D). Notably, early after initiation of CPA treatment (two times CPA therapy) expression levels of Thy-1, Oct4, Sox2 and Nanog were found to be transiently decreased to low expression levels, indicating transient reduction of stemness. Moreover, after long term treatment (6 times of CPA therapy), expression levels of all four pluripotency markers rose in the resistant tumors (HUH-REISO) again.

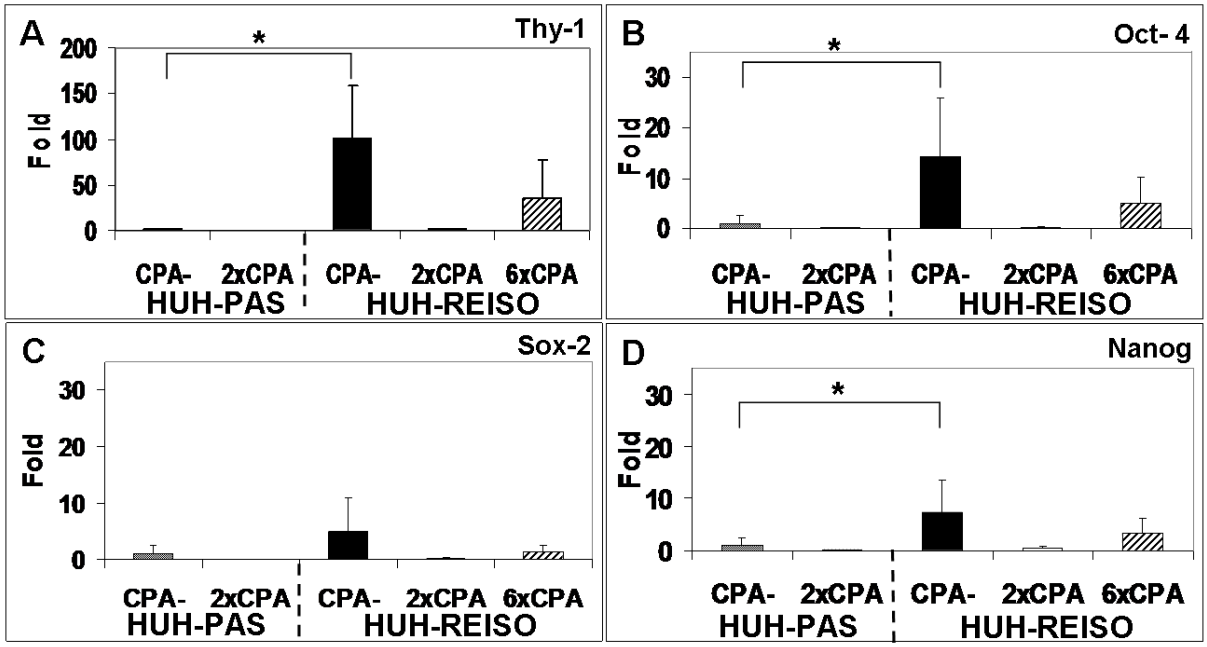

Figure 11: Expression of the plasticity markers Thy-1, Oct-4, Sox-2 and Nanog in tumor tissue

Influence of CPA treatment on expression levels of (A)Thy-1, (B) Oct-4, (C) Sox-2 and (D) Nanog was determined in tumor tissue by qRT-PCR analysis without (CPA-) and in tumor tissue after two (2xCPA+; HUH-PAS, HUH-REISO) and six (6xCPA+; HUH-REISO) CPA treatments (n=5 for each column). CPA-sensitive HUH-PAS tumors would not survive a 6xCPA- long-term treatment in sufficient extent required for analysis. Statistic evaluation was performed using the Wilcoxon-Mann-Whitney test. $P< 0.05$ was considered as significant and indicated by *.

3.9 Expression profiles of Notch-1, Notch-3 and HES-1

Passaged (HUH-PAS) and resistant (HUH-REISO) tumor bearing mice were treated by metronomic CPA therapy. Interestingly, Notch-1 expression (Figure 12 A) was conversely regulated in comparison to Thy-1, Oct-4, Sox-2 and Nanog. Significant increase of Notch-1 (about 3-fold) expression was detected only in *in vivo* passaged tumors ($p=0.028$) after two times of CPA treatment. Regulation of Notch-1 in already resistant tumors was not observable. Even after six chemotherapy treatment cycles, Notch-1 expression levels stayed constant. However, expression of HES-1, a target gene of the Notch pathway, was upregulated after two CPA-treatments in passaged and in resistant tumors. In HUH-PAS tumors, levels of HES-1 were 2.3 fold higher ($p=0.0090$), in HUH-REISO tumors 2.4 fold higher ($p=0.0143$) (Figure 12 B), if

compared with the corresponding non-treated counterparts. After six treatments, HES-1 expression levels sank to the levels of untreated tumors. HES-1 expression levels were about 2-fold higher in *in vivo* passaged tumors, compared to *in vivo* resistant tumors, independent of the treatment. Congruent to Notch-1 regulation, significant increase of Notch-3 expression levels (about 3.7 fold) were detected in *in vivo* passaged tumors ($p=0.0247$) after two times of CPA treatment (Figure 12 C). In resistant tumors an increased level about 2-fold ($p=0.0446$), which appeared after two treatments, disappeared after further four treatments.

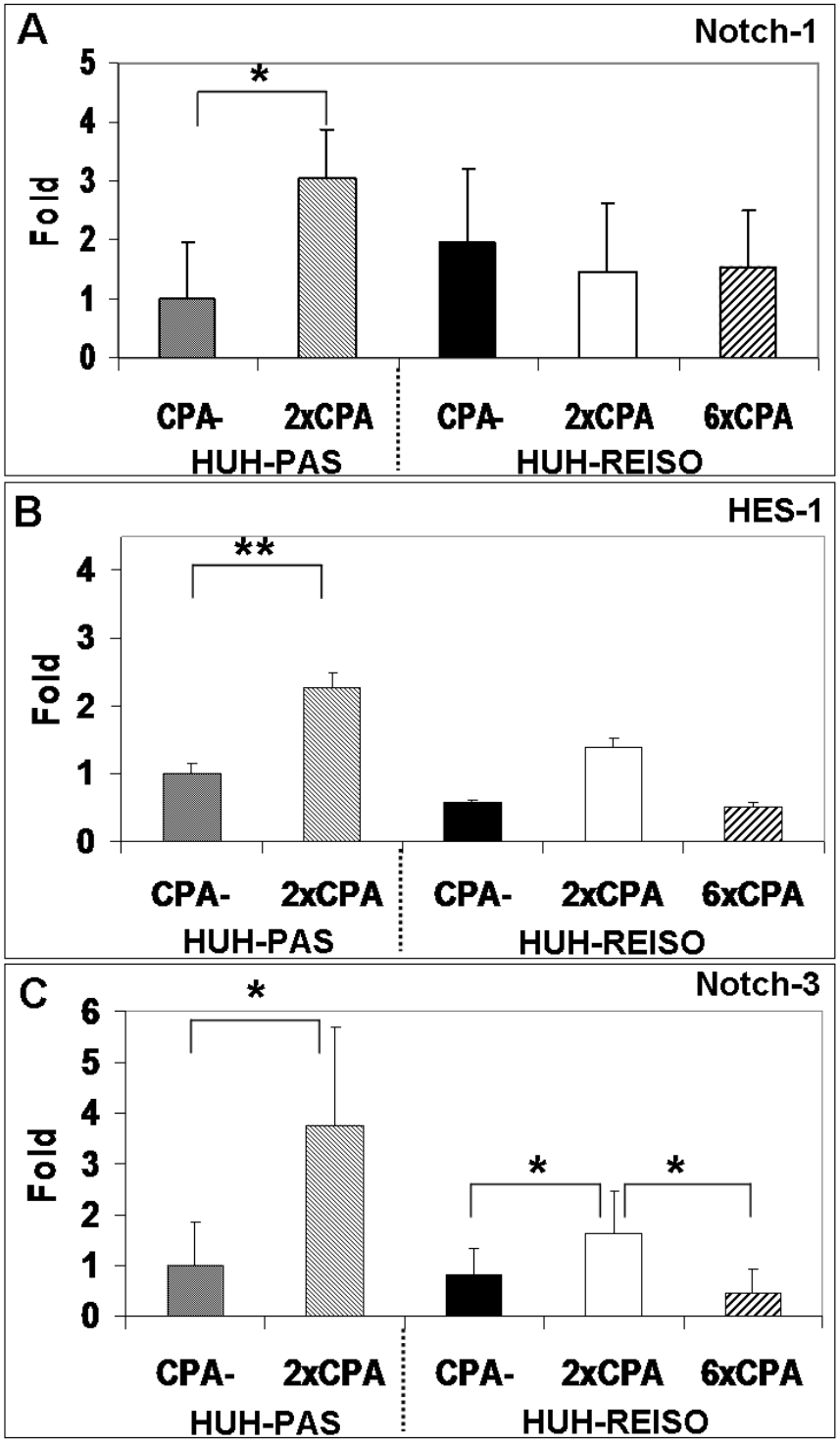

Figure 12 Expression of Notch-1, Notch-3 and its downstream target HES-1 in tumor tissue

Influence of CPA treatment on expression levels of Notch-3, Notch-1 and its downstream target HES-1 were determined in tumor tissue by qRT-PCR analysis before and after two CPA-treatments (HUH-PAS and HUH-REISO) and further four treatments in the case of HUH-REISO (n=5). (A) In contrast to significant induction of Notch-1 expression by two CPA therapies in passaged tumors (HUH-PAS), Notch-1 expression levels in chemoresistant

tumors (HUH-REISO) remained not significantly altered even after four further CPA-treatments. Initial expression levels of Notch-1 were not significantly different.
(B) HES-1 expression levels were detected to be significantly induced after two treatments for passaged (HUH-PAS) and chemoresistant tumors (HUH-REISO). Initial expression levels and expression levels after two CPA-treatments remained significantly low compared to tumors grown from *in vivo* passaged cells (HUH-PAS). After four further treatments, expression levels again reached initial HES-1 expression in chemoresistant tumors (HUH-REISO).
(C) Notch-3 showed in both groups HUH-PAS ($p=0.0247$) and HUH-REISO ($p=0.0446$) significantly upregulated levels after two times of CPA therapy. After additional four CPA treatments, level of Notch-3 in HUH-REISO dropped back on base levels.

3.10 Anchorage independent growth of HUH-wt, HUH-PAS and HUH-REISO spheroids

For characterization of cell dependency on essential matrix signaling, the capacity for anchorage-independent growth was tested by their ability to form colonies in soft agar. Multicellular spheroids were counted 42 days after embedding the single cell suspension (5,000 cells/well) in solid medium (Figure 13). The lowest spheroid forming capacity was detected for the HUH-wt, which developed only 9 spheroids out of 5,000 seeded cells. Interestingly, cells from HUH-PAS exhibited a 15-fold increased capacity (140 spheroids / 5,000 seeded cells) for anchorage-independent growth, in comparison to the original cell line. Spheroid forming capacity of HUH-REISO cells, building around 104 spheroids / 5,000 seeded cells, was 11-fold increased compared to HUH-wt but lower compared to HUH-PAS. No significant differences spheroid forming capacity was observed between resistant and non-resistant tumor cells, as only HUH-wt built far less spheroids than the other two cell lines.

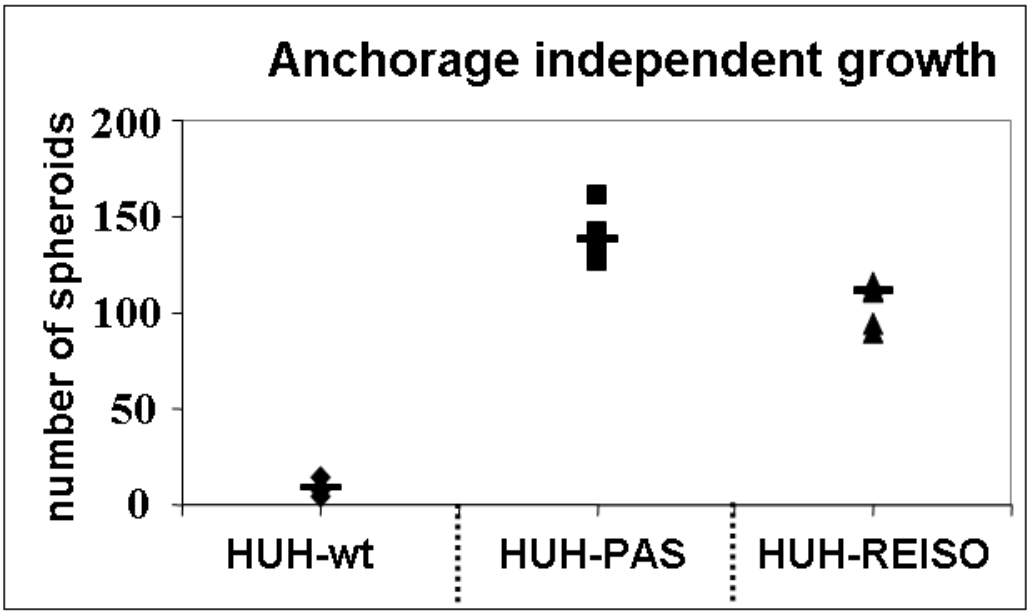

Figure 13 Anchorage independent growth. Spheroid forming capacity was determined by counting multicellular spheroids under the microscope (horizontal bar: median), resulting in low spheroid forming capacity (<20 spheroids/well) for parental HUH-7 cells (HUH-wt) and significantly increased forming potential in cells, which were derived from xenografts (HUH-PAS and HUH-REISO).

Nevertheless, the spheroids differed in their appearance. The parental HUH-wt cells (Figure 14 A) and *in vivo* passaged cells (Figure 14 B) built up very compact and homogeneous spheroids. In contrast, spheroids from the resistant tumor cells (Figure 14 C) were characterized by cavities within the spheroids. These findings could be consolidated by HE staining of 10 µm cryosections of spheroids. HUH-wt spheroids (Figure 14 D) and HUH-PAS spheroids (Figure 14 E) showed uniform and continuous tissue without cavities, whereas HUH-REISO spheroids (Figure 14 F) presented a sponge-like structure inside the spheroids.

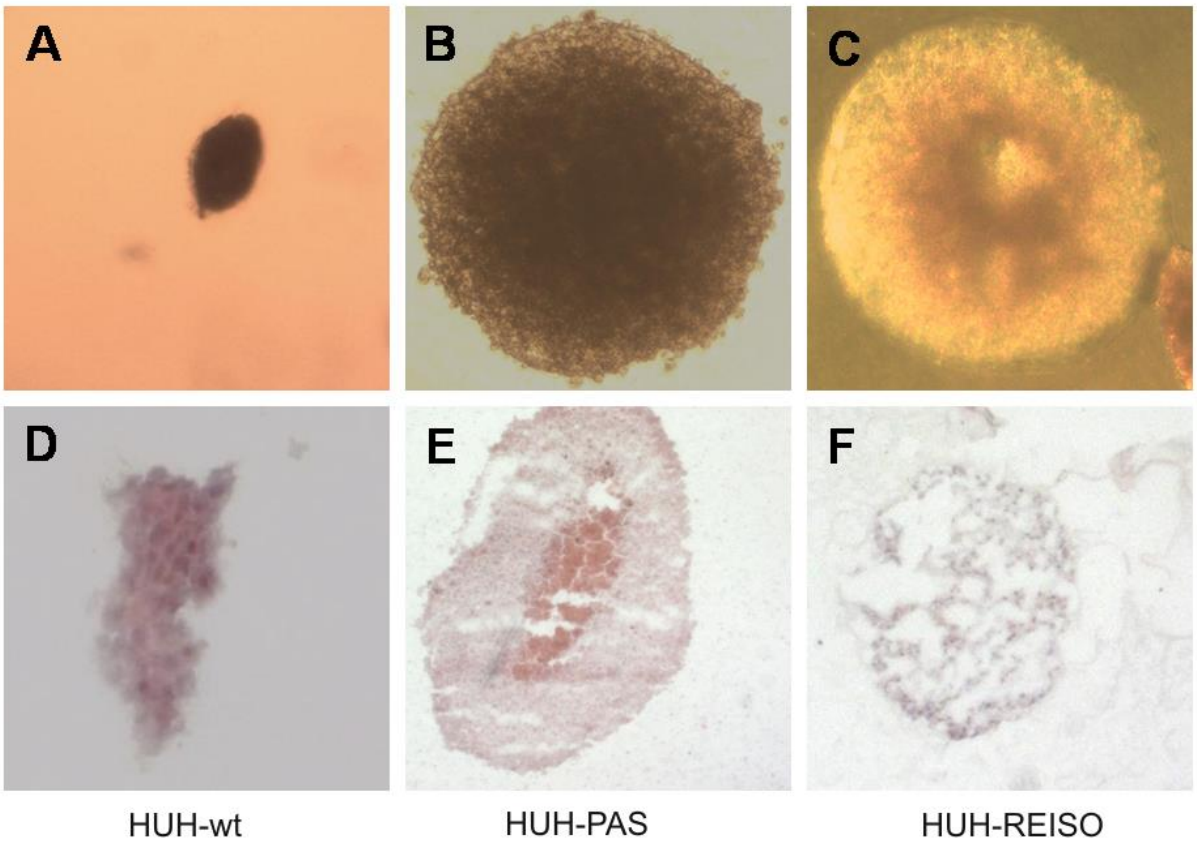

Figure 14: Anchorage independent growth. Multicellular spheroids grew from a single cell suspension of (A) parental HUH-7 cells (HUH-wt), (B) *in vivo* passaged HUH7 cells (HUH-PAS) and (C) chemoresistant cells (HUH-REISO) in low melting agarose for 42 days and pictures were taken under a phase contrast microscope. Spheroid tissue organization was detected by H/E staining of cryoslides. You can see in (D) parental HUH-7 cells (HUH-wt), in (E) *in vivo* passaged HUH7 cells (HUH-PAS) and in (F) chemoresistant cells (HUH-REISO).

3.11 Endothelial trans-differentiation *in vitro*

To evaluate the potential of tumor cells to transdifferentiate into an endothelial phenotype, a tube formation assay (Figure 15) was performed. At first, HUH-wt, HUH-PAS, and HUH-REISO cells were pre-cultured under conventional conditions (Figure 15 A-C) or under a thin layer of solid medium (“agarose overlay”, Figure 15 D-F) for six weeks. In this diffusion controlled environment [38], supply with nutrients and oxygen and moreover, dilution of autocrine and paracrine factors is limited, compared to conventional cell culture systems. After the pre-culture, the six different cell culture groups were subjected to a conventional matrigel assay (Figure 15 A-F). Only HUH-REISO cells, pre-cultured by agarose overlay, showed enough plasticity to

form endothelial like tubes within 4 hours (data not shown). After 24 h, the network was fully trained in this group (Figure 15 F), whereas HUH-wt (Figure 15 D) and HUH-PAS (Figure 15 E) cells showed no striking tube formation. Moreover, tube formation was not detectable in all three tumor cell groups pre-cultured under conventional conditions (Figure 15 A-C).

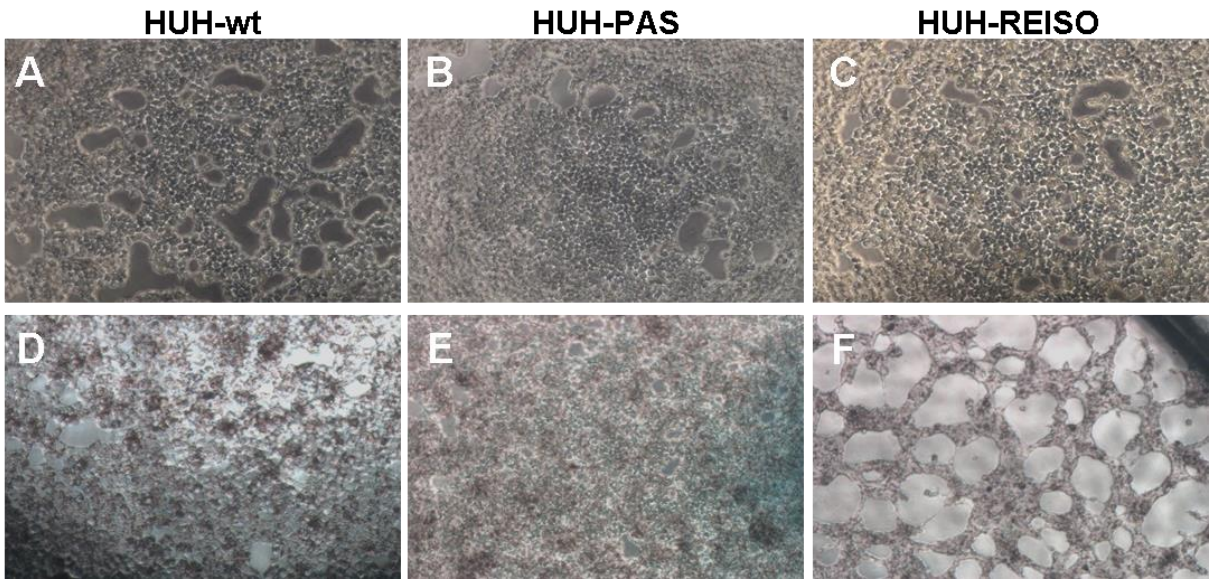

Figure 15 Tube formation assay. Tumor cells were seeded on matrigel after conventional cell culture (21% Oxygen / 37 °C) or after a 42 days culture in a diffusion limited environment with reduced oxygen and nutrient supply. Pictures were taken 24 hours after plating. (A) Parental HUH7 (HUH-wt), (B) *in vivo* passaged (HUH-PAS) and (C) chemoresistant (HUH-REISO) cells derived from conventional cell culture did not show tube formation, whereas in the case of cells, derived from the diffusion limited environment, the (F) chemoresistant tumor cells (HUH-REISO) showed significant tube formation potential in the matrigel assay, in comparison to (D) HUH-wt and (E) HUH-PAS (n=5).

Quantification of tube formation in matrigel was performed via software based analysis (Figure 16 A-J). Comparison of HUH-wt, HUH-PAS, and HUH-REISO (all pre-cultured by agarose overlay) revealed a far higher number of branching points (Figure 16 G) and tubes (Figure 16 H), a very extended length of skeleton (Figure 16 I), and a decreased amount of confluent areas without tube formation (Figure 16 J) for HUH-REISO cells.

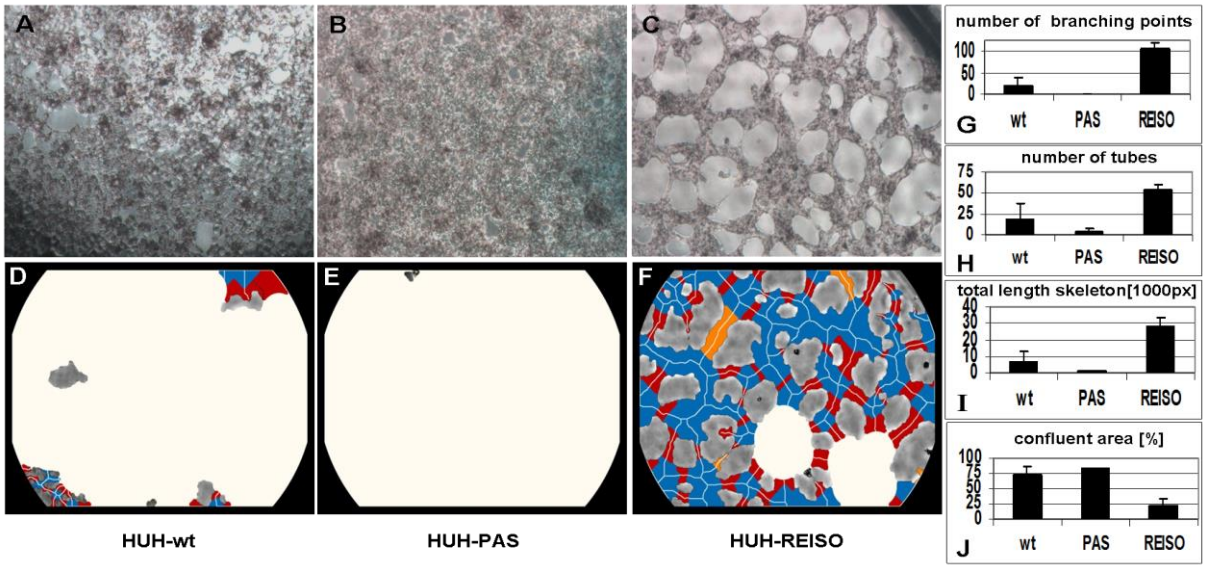

Figure 16 Software based analysis of matrigel assay. The software based analysis system projected a mask on pictures from transmitted light microscopy of matrigel assay (same pictures as described in Fig. 9D, E and F). In white are confluent areas, in blue are nodular structures coloured and built counted tubes with orange and red coloured areas. The tube skeleton is indicated in the thin white lines and their crossing points are defined as branching points. As HUH-wt (A) and HUH-PAS (B) revealed no tube formation, the projected mask is hardly coloured (D and E). HUH-REISO (C) showed low amount of confluent white area and accordingly contained all other aspects of functional tube formation (F). Software based analysis of pictures revealed a significantly increased (G) number of branching points, (H) overall number of tubes and (I) total length skeleton in chemoresistant cells (HUH-REISO) in comparison to both control cell lines (HUH-wt and HUH-PAS). Consequently, (J) the total confluent area was significantly decreased for HUH-REISO (n=3).

Furthermore, expression levels of endothelial markers (CD31/PECAM-1, ICAM-2, VEGFR2, VE-cadherin and vWF) of agarose overlay HUH-REISO cells, showing positive tube formation, were compared to the corresponding standard culture HUH-REISO (Figure 17 A and B). Expression levels were determined after the matrigel assay. In agarose overlay HUH-REISO cells, ICAM-2 ($p=0.009$) (Figure 17 A), as well as CD31/PECAM-1 ($p=0.028$) (Figure 17 B) were significantly upregulated. Expression of the other endothelial markers was not detectable in HUH-REISO under any culture condition.

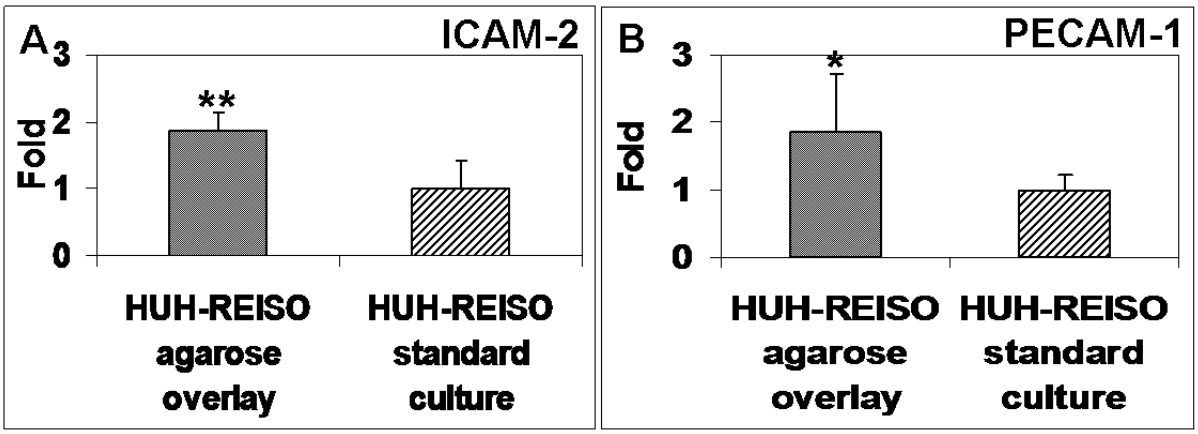

Figure 17 Expression of endothelial markers after hypoxic conditions. A qRT-PCR analysis, performed after the tube formation assay on the endothelial markers (A) ICAM-2 and (B) PECAM-1/CD31, revealed significantly increased expression levels for cells derived from the diffusion limited environment culture compared to conventional cultured cells, which did not show tube forming potential (n=6).

4 DISCUSSION

4.1 The HCC xenograft mouse model

In the present thesis, acquired *in vivo* chemoresistance against metronomic cyclophosphamide (CPA) treatment was studied in a human hepatocellular carcinoma HUH7 xenograft mouse model. During treatment, a two phase development of tumor progression was observable: In the beginning of treatment (response phase), tumor progression was significantly decreased, indicated by constant tumor volume for about 75 days. In the following second phase (escape phase), tumor volume increased with a tumor volume doubling time of 3.5 days despite ongoing therapeutic intervention (Figure 3).
Viable tumor cells were extracted from such resistant tumors (HUH-REISO), whereas control cells (HUH-PAS) were obtained from *in vivo* passaging HUH7 tumor cells without CPA treatment. Subsequently, HUH-PAS and HUH-REISO were characterized and identified in terms of cell morphology and representative human epidermal growth factor (EGF receptor) expression for their human origin (Figure 4).

4.2 No resistance *in vitro*, no well-known mechanism

Interestingly, *in vivo* chemoresistant HUH-REISO did not manifest their drug resistant phenotype in a two-dimensional monolayer culture in presence of *in situ* activated CPA (Figure 8). However, mechanisms like upregulated detoxicating enzymes, efflux pumps, increased DNA repairing, and deficient apoptosis are not limited to the *in vivo* situation and should be also evident *in vitro*. In addition, significant changes in macroscopic appearance and tumor tissue organization of chemoresistant tumors indicate resistance mechanisms, which were only executed in the *in vivo* situation.

4.3 Manifested chemoresistance directly after re-implantation

An endogenous imprinted component for *in vivo* chemoresistance was obvious, as the chemoresistant phenotype of isolated tumor cells was immediately manifested

again after re-implantation and reapplied chemotherapy. Differences in experimental setup were avoided by a setting where every mouse bore two tumors. *In vivo* passaged only HUH-PAS were implanted into the left flank and chemoresistant HUH-REISO into the right flank. In the re-implantation experiment, chemoresistance was manifested in HUH-REISO lacking the response phase against administered CPA. In contrast, HUH-PAS, which had only been adjusted to the *in vivo* environment but not to the CPA treatment, remained sensitive (Figure 9) in a response phase. This special experimental setup also proved sufficient activation of CPA, as HUH-PAS were sensitive against therapy.

4.4 Detoxification of CPA by ALDH-1

The qRT-PCR assay on *in vivo* samples revealed no significant difference in basal expression of the detoxification enzyme ALDH-1 (Figure 10), which converts aldophosphamide into carboxyphosphamide. ALDH-1 expression was detected to be significant upregulated *in vivo* during therapeutic pressure. However, the extent of upregulation was not significantly different in chemosensitive and chemoresistant tumors. The detected chemosensitivity of HUH-PAS exclude resistance by unspecific selection processes *in vivo*, which might change cellular properties independently of therapeutic pressure [39, 40].

4.5 Blood-flow and supplementation in tumors

As metronomic CPA treatment is known to suppress tumor angiogenesis [25], functional blood flow analysis was performed, revealing blood flow in a part of the newly formed cavities of chemoresistant tumors (Figure 5 F). In contrast to untreated animals, blood flow was not obligatory co-localized with immunohistochemical detected laminin and mouse PECAM-1/CD31 signal (Figure 7 B). Further analysis on human vessel markers revealed the presence of cells expressing human PECAM-1/CD31 (Figure 7 M/N) within the tumor, indicating plasticity of the tumor cells and initiation of differentiation towards the endothelial lineage. This differentiation was observed only in HUH-REISO. In HUH-PAS the CPA therapy led to a deletion of murine vessels (Figure 7 H), while the capacity of building new human vessels was

not observed. As HUH-REISO showed no diminished blood-flow (Figure 6) and also a supplementation of destroyed murine vessels by human endothelial cells, resistance is partly caused by a better blood-supplementation due to the higher plasticity of HUH-REISO. Better blood-supplementation leading to higher drug delivery into the tumor presumably requires also other detoxification mechanisms for the resistance. The higher levels of ALDH-1 in HUH-REISO (6xCPA,Figure 10) are consistent with this hypothesis. Therefore, further changes in the microenvironment and proteome of the resistant tumor cells remain to be examined in future work.

4.6 Anchorage independent growth and spheroid morphology

Plasticity becomes often apparent in combination with the capacity of self-renewal and potential of anchorage independent growth, frequently assessed in spheroid building capacity assays [41, 42]. In such an assay, no significant differences between resistant and non-resistant tumor cells could be observed (Figure 13). However, this fact is not surprisingly at all as there is only rare human tissue as renewable and regenerative as the liver tissue. Consequently, all cell lines of our liver cancer showed a good potential of anchorage independent growth, especially in the selected cells of *in vivo* pressure. Nevertheless, a big difference was observable between the different cell lines looking into the inner area of the spheroids. In contrast to spheroids derived from HUH-wt (Figure 14 A/D) or from *in vivo* passaged HUH-PAS cells (Figure 14 B/E), spheroids formed by HUH-REISO cells revealed the formation of cavities and tubular structures (Figure 14 C/F). This indicated cellular changes, which differed from the environmental conditioning of *in vivo* passaging. The consequent sponge-like growth (both in spheroids and in tumors) might also ensure an easier supplementation of HUH-REISO tissue with nutrients and oxygen than in compact HUH-PAS and HUH-wt tissue. Thus, for experiments HUH-PAS cells were used as an adequate control, to characterize development of chemoresistance *in vivo*.

4.7 Stemness and plasticity makers by qRT-PCR

Taking the detected plasticity into account, HUH-PAS and HUH-REISO *in vivo* tumors were analyzed for expression profiles of markers, which are highly expressed in embryonic cells and described in recent papers about tumor initiating cells [43-45]. Expression of Oct-4 plays a crucial role in maintaining pluripotency in stem cells [43]. Additionally, Sox-2 and Nanog expression contribute to plasticity, self-renewal and stemness [44]. Especially, in the context of HCC tumor stem cell research, Thy-1 expression is discussed as one crucial regulator of stemness and its upregulation is described in the context of chemoresistance [45]. In the absence of chemotherapy *in vivo* (-CPA, Figure 11 A-D), qRT-PCR revealed significantly increased expression levels of Thy-1, Oct-4, Sox-2 and Nanog in the re-implanted chemoresistant HUH-REISO tumors compared with the *in vivo* passaged HUH-PAS control tumors. This indicates an inherent difference of the chemosensitive HUH-PAS and chemoresistent HUH-REISO tumors, with an enrichment of tumor cells with a reprogrammed, embryonic-like status for HUH-REISO. To monitor the response of HUH-REISO tumors towards CPA treatment with time, qRT-PCR analyses were performed also after 2x CPA and 6x CPA treatment. HUH-PAS tumors were analyzed in parallel, but after 2 treatments only. The late time point (6x CPA) was not evaluated due to the lack of tumor outgrowth on the one hand, or upon outgrowth conversion into a REISO-type resistant tumor on the other hand. At the earlier (2xCPA) time point, resistance was not yet established for HUH-PAS (day 14, no tumor outgrowth,Figure 9). *In vivo* passaging alone generated only few cells with pluripotent capacities (HUH-PAS, CPA-), but these cells differentiated very fast or got lost under therapeutic pressure (HUH-PAS, 2xCPA). In contrast, HUH-REISO generate tumor tissue containing a pluripotent sub-population (Figure 11, -CPA). Upon CPA treatment, HUH-REISO tumors continue to grow, but partly lost their pluripotent stem cell population during the acute response to the first two treatments (Figure 11, HUH-REISO, 2xCPA), presumably by differentiation. However, chemoresistent tumors were able to regenerate the pool of stem cells (Figure 11, HUH-REISO, 6xCPA) and reached a “steady-state” with stemness markers again. Based on these stemness marker results, recent papers [46-49] and my results regarding Notch-pathways, I propose the hypothesis shown in Figure 18.

4.8 Notch-1 the important factor in keeping pluripotency

In line with literature [46], the process of reprogramming was connected to induction of Notch-1 expression, as a first response to chemotherapeutic pressure (Figure 12 A). Induction of Notch-1 leads to the expression of GIMAP5 [46], which is anti-apoptotic and has potential to improve cell survival. ALDH-1 was simultaneously induced (Figure 10) and led to cell survival under therapeutic pressure. Furthermore, induction of HES-1, which is a downstream target of Notch-1, was observable (Figure 12 B). HES-1 belongs to the basic helix loop helix family of transcription factors and is described by Kageyama et al. as a crucial factor in many tissues to maintain the status of pluripotency [47]. Notch-1 and HES-1 were only upregulated in the response phase of therapy, indicating an initial key factor in this process. In the escape phase of already chemoresistant tumors, Notch-1 was steadily regulated under chemotherapeutic pressure, indicating that Notch-1 was essential for the preservation of the reprogrammed status, once Thy-1, Oct-4, Sox-2 and Nanog provides pluripotency and self-renewal.

4.9 Notch-3 the important factor in endothelial trans-differentiation

Surprisingly, after two treatments with CPA, expression levels of Thy-1, Oct-4, Sox-2 and Nanog were decreased in HUH-REISO (Figure 11 A-D), indicating a process of differentiation, which obviously antagonize further enrichment of this subpopulation at this point of treatment. This correlated with the induction of Notch-3 expression. The Notch-3 pathway is described as an important signalling pathway in the development of vascularization. N. Lawson et al. [48, 49] showed the important role of Notch-3 in arterial cell fate during blood vessel development. However, after prolonged CPA treatment, expression levels of all pluripotency markers recovered. The initial expression profile of Notch-3 and the profile of Thy-1, Oct-4, Sox-2 and Nanog pointed to an adaptation process, as a response to acute chemotherapeutic pressure.

4.10 A pool of pluripotent cells

Obviously, differentiation was repressed again after adaptation and the balance returned to enrichment of pluripotent cells. An important step to the *in vivo* chemoresistance in our model was therefore the development of a pool of cells, which reveal increased levels of pluripotency markers and obviously help to overcome chemotherapeutic pressure by initiation of differentiation (Figure 18). In contrast to chemoresistant tumors, the CPA therapy in chemosensitive tumors led to the induction of differentiation processes and cell death, which in the beginning of treatment nearly flushed out the whole pool of pluripotent tumor cells. Recovering of this pool took long time (growth delay phase Figure 9) and led, beside other mechanisms, in the end to resistance (Figure 3).

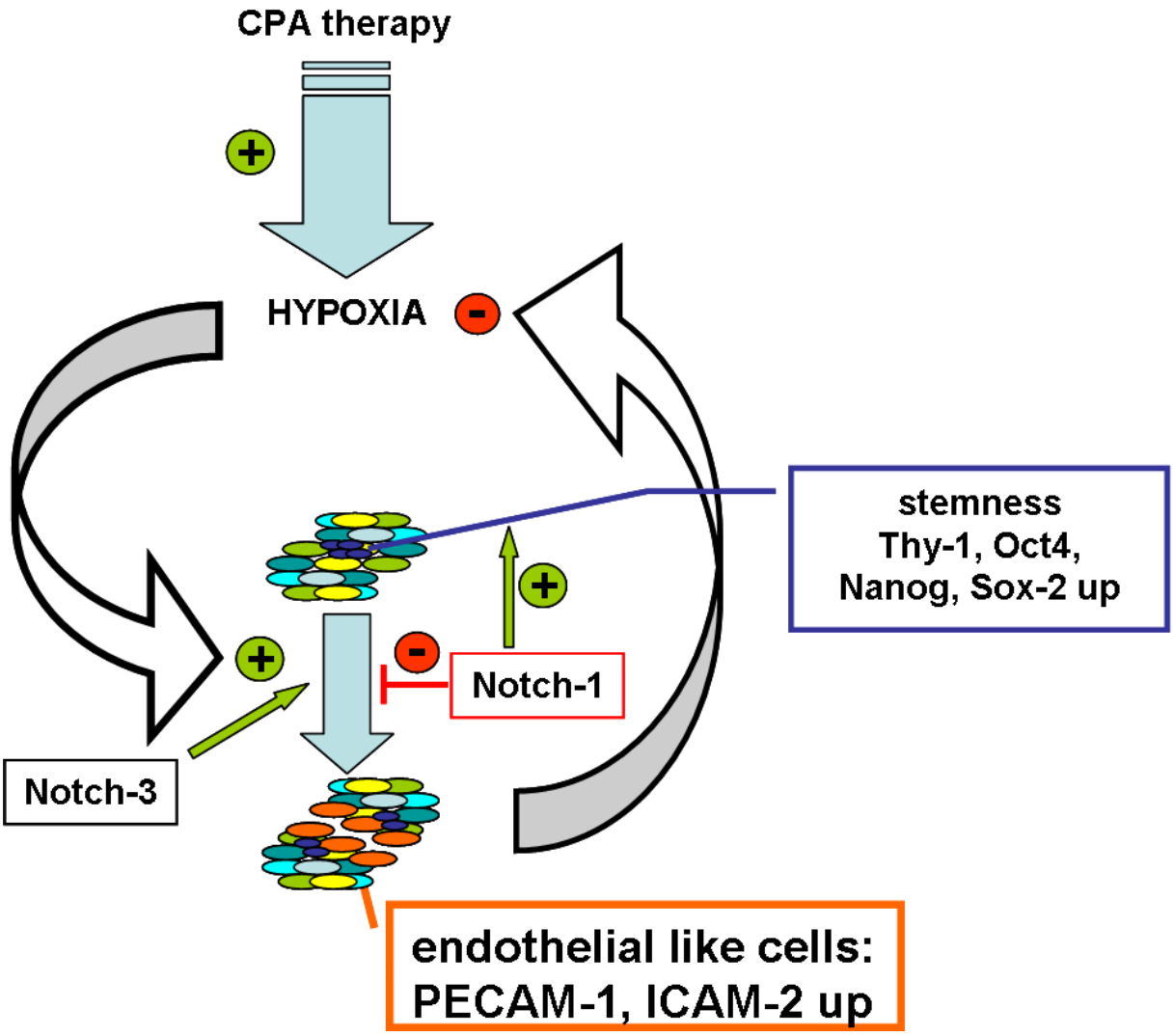

Figure 18 Acquired chemoresistance towards metronomic CPA therapy – a hypothetical model of the equilibrium between stem cells and endothelial like cells in HUH-REISO. During therapeutic pressure tumor cells acquire stepwise pluripotency. Reprogramming is associated with regulations of the Notch-pathway (Notch-1), resulting in enrichment of cells with increased expression levels of Thy-1, Oct-4, Sox-2 and Nanog. This pool of cells is the basis for increased adaptiveness of the tumor to therapy effects as hypoxia. Differentiation to a functional endothelial like phenotype, connected with tissue reorganization, counteracts antiangiogenic therapy. Finally, in the chemoresistant tumors exists an equilibrium between differentiation and self-renewal. In contrast to chemoresistant tumors, induction of Notch-3 expression in chemosensitive tumors leads to the induction of a differentiation process, which nearly flushes out the whole pool of pluripotent tumor cells.

4.11 Endothelial trans-differentiation triggered by oxygen limitation

This differentiation process, resulting in the reorganization of tumor tissue, helped tumors to escape the metronomic treatment. To investigate the trigger, which caused differentiation, HUH-wt, HUH-PAS, and HUH-REISO cells, were pre-cultured in an *in vitro* cell culture system, which mimics several features of solid tumors under therapeutic pressure. In a following matrigel tube formation assay, usually performed for angiogenesis studies [50], HUH-REISO cells showed tube formation capacity (Figure 15 F), whereas cells pre-cultured under conventional conditions showed no functionality (Figure 15 C). Importantly, HUH-wt and HUH-PAS revealed no tube formation potential, independently of pre-culture conditions. Obviously, initiation of differentiation only took place in an environment, which was characterized by limitation of oxygen supply and simultaneous diffusion limitation of paracrine and autocrine factors. In recent studies, the phenomena of tumor cell tube formation on matrigel was detected e.g. for glioblastoma, breast cancer [51] and multiple myeloma [52]. In several studies, the feature of tube formation was independent from the expression of endothelial markers (vascular mimicry) [53]. However, in the case of HUH-REISO cells, tube formation was associated with induction of the endothelial genes PECAM-1/CD31 and ICAM-2 (Figure 17 A and B). In contrast, other endothelial marker genes as vWF, VEGFR2 and VE-cadherin were neither expressed, nor regulated. Expression of endothelial genes was published by Bussolati et al. and Bruno et al., who detected induction of endothelial marker expression, derived from tumor initiating cells (tumor stem cells) by treatment via VEGF [54] or after xenografting [55]. Apparently, HUH-REISO cells, or at least a subpopulation acquired a reprogrammed status characterized by enormous plasticity. This pool of cells reacted on environmental requirements by initiation of differentiation in specialized cells to maintain a balanced tumor microenvironment, ensured sufficient oxygen and nutrient supply and finally counteracted metronomic therapy.

It remains to be investigated whether the plasticity as observed with HUH7 is especially pronounced with HCC or other tumors. In this regard, recent interesting observations from normal liver organogenesis [56]. For long time it had been assumed that the endoderm generates the hepatocytes, while the mesoderm generates the liver endothelial cells. Now it was discovered that the endodermal cells

can generate approximately 15% of the liver endothelial cells, demonstrating a special plasticity in endodermal liver progenitor cells.

5 CONCLUSION AND OUTLOOK

In conclusion, studying the escape mechanism towards metronomically applied CPA therapy in a HCC xenograft model revealed a multistep process, going beyond unspecific enrichment of a certain subpopulation by the *in vivo* tumor environment. First step of this process was the enrichment of detoxicating enzyme ALDH-1 in combination with upregulation of the Notch1-pathway and its protective downstream effector proteins. As a result, therapy could be overcome by this mechanism. The second step was a selection process of pluripotent, stem cell marker expressing cells with pluripotent trans-differentiation capacities. Their capacities included that these cells have increased endothelial trans-differentiation *in vivo* and *in vitro*. Functionality of such endothelial-like cells helped resistant tumors to overcome anti-angiogenic therapy and was the most important finding of this study. Further examinations, on how modification of Notch signalling may impact cell plasticity and differentiation remain to be explored in future. Also co-medication studies *in vivo* with CPA in combination with Notch-antibodies or agents which interrupt Notch-pathway could be enlightning. Of course, a proteomics approach of the different cell lines would be a perfect tool for further examinations.

6 SUMMARY

Chemotherapeutic treatment of hepatocellular carcinoma often leads to chemoresistance during therapy or upon relapse of tumors. For the development of better treatments, a better understanding of biochemical changes in the resistant tumors is needed. Therefore, especially *in vivo* models are very important tools to generate standardized cell-material, which can be examined by high throughput techniques. Thus, it should be possible to find new targets for therapy or even for diagnostic. This thesis focusses on the characterization of the *in vivo* chemoresistant human hepatocellular carcinoma HUH-REISO established from a metronomically cyclophosphamide (CPA) treated HUH7 xenograft mouse model.

First step of the work was the establishment of the xenograft mouse model. SCID mice bearing subcutaneous HUH7 tumors were treated i.p. with 75 mg/kg CPA every six days. After 10 weeks of response to the therapy, the tumor growth relapsed and tissue grew with very fast doubling time again, despite of ongoing treatment. This aggressive manner of growth under therapy could be also observed in a re-implantation study where the reisolated CPA chemoresistant HUH-REISO tumors grew without a lag phase, indicating an endogenous imprinted component. To evaluate this, tumors were examined by immunohistochemistry, a functional blood-flow Hoechst dye assay, and qRT-PCR for ALDH-1, Notch-1, Notch-3, HES-1, Thy-1, Oct-4, Sox-2 and Nanog mRNA levels.

Histochemical analysis of HUH-REISO tumors revealed significant changes in host vascularization of tumors and especially in expression of the tumor-derived human endothelial marker gene PECAM-1/CD31 in HUH-REISO in comparison to parental HUH-7 cells and *in vivo* passaged HUH-PAS cells (*in vivo* grown without chemotherapeutic CPA pressure). The pronounced network of host murine vascularization in parental HUH-7 tumors was completely substituted by a network of human and murine vessel-like structures in HUH-REISO tumors under therapy.

In addition, cell lines of these tumors were analyzed in endothelial trans-differentiation studies on matrigel. In those studies with limited oxygen and metabolite diffusion, followed by a matrigel assay, only the chemoresistant HUH-REISO cells exhibited tube formation potential and expression of human endothelial markers ICAM-2 and PECAM-1/CD31. Such a trans-differentiation capacity requires a lineage

of cells with pluripotent capacities like so called tumor stem cells. Indeed, I could show in a comparative study on stemness and plasticity markers that Thy-1, Oct-4, Sox-2 and Nanog were upregulated in resistant xenografts. Furthermore, under therapeutic pressure by CPA, tumors of HUH-PAS and HUH-REISO displayed regulations in Notch-1 and Notch-3 expression, which I could also show by qRT-PCR. Notch-1 raised in HUH-PAS under therapeutic pressure, meanwhile it was conversely regulated in comparison to Thy-1, Oct-4, Sox-2 and Nanog in HUH-REISO. In both groups Notch-3 was inducible by 2 times CPA treatment and fell back on base level after further four therapeutic cycles in HUH-REISO.

To conclude all these finding: chemoresistance of HUH-REISO was not manifested under standard *in vitro,* but only under *in vivo* conditions. HUH-REISO cells showed increased pluripotent capacities and the ability of trans-differentiation to endothelial like cells *in vitro* and *in vivo*. These cells expressed typical endothelial surface marker and functionality. Although the mechanism behind chemoresistance of HUH-REISO and involvement of plasticity remains to be clarified, we hypothesize that the observed Notch regulations and upregulation of stemness genes in resistant xenografts are involved in the observed cell plasticity.

7 APPENDIX

7.1 Abbreviations

Act-B	-	Beta actin
ALDH-1	-	Aldehyde dehydrogenase
cDNA	-	copy deoxyribonucleic acid
CD XY	-	Cluster of differentiation protein number xy
CO_2	-	Carbon dioxide
CPA	-	Cyclophosphamide
CYP2B1	-	Cytochrome P450, family 2, subfamily B, polypeptide 1
DAPI	-	4′,6-Diamidin-2-phenylindol
DMEM	-	Dulbecco's modified eagle medium
EDTA	-	Ethylenediamine tetra acetic acid
EGF	-	Epidermal growth factor
EGF-R	-	Epidermal growth factor receptor
FACS	-	Fluorescence-activated cell sorting
FBS	-	Fetal bovine serum
FGF	-	Fibroblast growth factor
G (needle)	-	Gauge
GAPDH	-	Glycerinaldehyde-3-phosphat-Dehydrogenase
HCC	-	Human Hepatocellular Carcinoma
HES-1	-	Hairy and enhancer of split-1
HE-stain	-	Hämatoxylin eosin staining
HIF-1α	-	Hypoxia inducible factor 1 alpha
HUH-7	-	Human Hepatoma cell line 7
ICAM-2	-	Intercellular adhesion molecule 2
i.p.	-	Intraperitoneal application
i.v.		Intravenous application
MTD		Maximum tolerated dose
NaCl	-	Sodium chloride
Oct-4	-	Octamer binding transcription factor 4
p / p-value	-	Probability of obtaining a test statistic result
PBS	-	Phosphate buffered saline

PCR	-	Polymerase chain reaction
PECAM-1/CD31	-	Platelet endothelial cell adhesion molecule
PFA	-	Paraformaldehyde
PIGF	-	Phosphatidylinositol-glycan biosynthesis class F protein
qRT-PCR	-	Quantitative realtime polymerase chain reaction
RNA	-	ribonucleic acid
SCID	-	Severe Combined Immunodeficiency
SD	-	Standard deviation
Sox-2	-	Sex determining region Y-box 2
Thy-1 / CD90	-	Thymocyte differentiation antigen 1
Tris	-	Trometamol
VE-cadherin	-	Vascular endothelial- cadherin
VEGF	-	Vascular endothelial growth factor
wt	-	wild-type

7.2 Publication

Marfels, C., Hoehn, M., Wagner, E., Günther, M. (2013) Characterization of in vivo chemoresistant human hepatocellular carcinoma cells with transendothelial differentiation capacities. *BMC Cancer* **13**, 176.

8 REFERENCES

1. Farazi, P.A. and R.A. DePinho, *Hepatocellular carcinoma pathogenesis: from genes to environment.* Nat Rev Cancer, 2006. **6**(9): p. 674-687.
2. Tanaka, M., et al., *Hepatitis B and C virus infection and hepatocellular carcinoma in China: a review of epidemiology and control measures.* J Epidemiol, 2011. **21**(6): p. 401-16.
3. Pang, R. and R.T.P. Poon, *Angiogenesis and antiangiogenic therapy in hepatocellular carcinoma.* Cancer Letters. **242**(2): p. 151-167.
4. Finn, R.S. and A.X. Zhu, *Targeting angiogenesis in hepatocellular carcinoma: focus on VEGF and bevacizumab.* Expert Review of Anticancer Therapy, 2009. **9**(4): p. 503-509.
5. Llovet, J.M., et al., *Sorafenib in advanced hepatocellular carcinoma.* N Engl J Med, 2008. **359**(4): p. 378-90.
6. Tannock, I.F., *The relation between cell proliferation and the vascular system in a transplanted mouse mammary tumour.* Br J Cancer, 1968. **22**(2): p. 258-73.
7. Goodall, C.M., et al., *Vascular patterns of four transplantable tumors in the hamster (Mesocricetus auratus).* Angiology, 1965. **16**(10): p. 622-5.
8. Hanahan, D. and J. Folkman, *Patterns and emerging mechanisms of the angiogenic switch during tumorigenesis.* Cell, 1996. **86**(3): p. 353-64.
9. Fidler, I.J., *Critical factors in the biology of human cancer metastasis: twenty-eighth G.H.A. Clowes memorial award lecture.* Cancer Res, 1990. **50**(19): p. 6130-8.
10. Weidner, N., et al., *Tumor angiogenesis and metastasis--correlation in invasive breast carcinoma.* N Engl J Med, 1991. **324**(1): p. 1-8.
11. Folkman, J., et al., *Isolation of a tumor factor responsible for angiogenesis.* J Exp Med, 1971. **133**(2): p. 275-88.
12. Schmidt, T. and P. Carmeliet, *Angiogenesis: a target in solid tumors, also in leukemia?* Hematology Am Soc Hematol Educ Program, 2011. **2011**: p. 1-8.
13. Adams, R.H. and K. Alitalo, *Molecular regulation of angiogenesis and lymphangiogenesis.* Nat Rev Mol Cell Biol, 2007. **8**(6): p. 464-78.

14. Ferrara, N., *VEGF-A: a critical regulator of blood vessel growth.* Eur Cytokine Netw, 2009. **20**(4): p. 158-63.
15. Nagy, J.A., A.M. Dvorak, and H.F. Dvorak, *VEGF-A and the induction of pathological angiogenesis.* Annu Rev Pathol, 2007. **2**: p. 251-75.
16. Phng, L.K. and H. Gerhardt, *Angiogenesis: a team effort coordinated by notch.* Dev Cell, 2009. **16**(2): p. 196-208.
17. Fontanini, G., et al., *Angiogenesis as a prognostic indicator of survival in non-small-cell lung carcinoma: a prospective study.* J Natl Cancer Inst, 1997. **89**(12): p. 881-6.
18. Fontanini, G., et al., *Microvessel count predicts metastatic disease and survival in non-small cell lung cancer.* J Pathol, 1995. **177**(1): p. 57-63.
19. Folkman, J., *Tumor angiogenesis: therapeutic implications.* N Engl J Med, 1971. **285**(21): p. 1182-6.
20. Hurwitz, H., et al., *Bevacizumab plus irinotecan, fluorouracil, and leucovorin for metastatic colorectal cancer.* N Engl J Med, 2004. **350**(23): p. 2335-42.
21. Sandler, A., et al., *Paclitaxel-carboplatin alone or with bevacizumab for non-small-cell lung cancer.* N Engl J Med, 2006. **355**(24): p. 2542-50.
22. Escudier, B., et al., *Phase III trial of bevacizumab plus interferon alfa-2a in patients with metastatic renal cell carcinoma (AVOREN): final analysis of overall survival.* J Clin Oncol, 2010. **28**(13): p. 2144-50.
23. Rini, B.I., et al., *Phase III trial of bevacizumab plus interferon alfa versus interferon alfa monotherapy in patients with metastatic renal cell carcinoma: final results of CALGB 90206.* J Clin Oncol, 2010. **28**(13): p. 2137-43.
24. Miller, K., et al., *Paclitaxel plus bevacizumab versus paclitaxel alone for metastatic breast cancer.* N Engl J Med, 2007. **357**(26): p. 2666-76.
25. Browder, T., et al., *Antiangiogenic scheduling of chemotherapy improves efficacy against experimental drug-resistant cancer.* Cancer Res, 2000. **60**(7): p. 1878-86.
26. Baguley, B.C., et al., *Inhibition of growth of colon 38 adenocarcinoma by vinblastine and colchicine: evidence for a vascular mechanism.* Eur J Cancer, 1991. **27**(4): p. 482-7.
27. Freissmuth, M. and S. Böhm, *61.2.1 Alkylierende Verbindungen und andere Quervernetzer*, in *Pharmakologie & Toxikologie*, S. Offermanns, Editor. 2012, Springer. p. 60ff.

28. Boddy, A.V. and S.M. Yule, *Metabolism and pharmacokinetics of oxazaphosphorines.* Clin Pharmacokinet, 2000. **38**(4): p. 291-304.
29. Hall, A.G. and M.J. Tilby, *Mechanisms of action of, and modes of resistance to, alkylating agents used in the treatment of haematological malignancies.* Blood Rev, 1992. **6**(3): p. 163-73.
30. Park, S., et al., *Beneficial effect of metronomic chemotherapy on tumor suppression and survival in a rat model of hepatocellular carcinoma with liver cirrhosis.* Cancer Chemotherapy and Pharmacology, 2010. **65**(6): p. 1029-1037.
31. Browder, T., et al., *Antiangiogenic Scheduling of Chemotherapy Improves Efficacy against Experimental Drug-resistant Cancer.* Cancer Research, 2000. **60**(7): p. 1878-1886.
32. Folkman, J., *Angiogenesis.* Annu Rev Med, 2006. **57**: p. 1-18.
33. Broxterman, H.J., J. Lankelma, and K. Hoekman, *Resistance to cytotoxic and anti-angiogenic anticancer agents: similarities and differences.* Drug Resist Updat, 2003. **6**(3): p. 111-27.
34. Emmenegger, U., et al., *Pharmacodynamic and pharmacokinetic study of chronic low-dose metronomic cyclophosphamide therapy in mice.* Mol Cancer Ther, 2007. **6**(8): p. 2280-9.
35. Thoenes, L., et al., *In vivo chemoresistance of prostate cancer in metronomic cyclophosphamide therapy.* J Proteomics, 2010. **73**(7): p. 1342-54.
36. Zhang, J., Q. Tian, and S.-F. Zhou, *Clinical Pharmacology of Cyclophosphamide and Ifosfamide.* Current Drug Therapy, 2006. **1**(1): p. 55-84.
37. Günther, M., *Cancer Therapy with Metronomically Scheduled Cyclophosphamide: Experimental Modalities within GDEPT and Tumor Escape Mechanisms.*, in *Fakultät für Chemie und Pharmazie* 2007, Ludwig Maximilian University: Munich.
38. Gunther, M., et al., *Effects of hypoxia and limited diffusion in tumor cell microenvironment on bystander effect of P450 prodrug therapy.* Cancer Gene Ther, 2006. **13**(8): p. 771-9.
39. Abe, T., et al., *Establishment and characterization of human urothelial cancer xenografts in severe combined immunodeficient mice.* Int J Urol, 2006. **13**(1): p. 47-57.

40. Mueller, M.M., et al., *Tumor progression of skin carcinoma cells in vivo promoted by clonal selection, mutagenesis, and autocrine growth regulation by granulocyte colony-stimulating factor and granulocyte-macrophage colony-stimulating factor.* Am J Pathol, 2001. **159**(4): p. 1567-79.
41. Gu, G., et al., *Prostate cancer cells with stem cell characteristics reconstitute the original human tumor in vivo.* Cancer Res, 2007. **67**(10): p. 4807-15.
42. Zhang, S., et al., *Identification and characterization of ovarian cancer-initiating cells from primary human tumors.* Cancer Res, 2008. **68**(11): p. 4311-20.
43. Hay, D.C., et al., *Oct-4 knockdown induces similar patterns of endoderm and trophoblast differentiation markers in human and mouse embryonic stem cells.* Stem Cells, 2004. **22**(2): p. 225-35.
44. Boyer, L.A., et al., *Core transcriptional regulatory circuitry in human embryonic stem cells.* Cell, 2005. **122**(6): p. 947-56.
45. Lu, J.W., et al., *Overexpression of Thy1/CD90 in human hepatocellular carcinoma is associated with HBV infection and poor prognosis.* Acta Histochem, 2011. **113**(8): p. 833-8.
46. Chadwick, N., et al., *Identification of novel Notch target genes in T cell leukaemia.* Mol Cancer, 2009. **8**: p. 35.
47. Kageyama, R., T. Ohtsuka, and K. Tomita, *The bHLH gene Hes1 regulates differentiation of multiple cell types.* Mol Cells, 2000. **10**(1): p. 1-7.
48. Lawson, N.D., et al., *Notch signaling is required for arterial-venous differentiation during embryonic vascular development.* Development, 2001. **128**(19): p. 3675-83.
49. Lawson, N.D., A.M. Vogel, and B.M. Weinstein, *sonic hedgehog and vascular endothelial growth factor act upstream of the Notch pathway during arterial endothelial differentiation.* Dev Cell, 2002. **3**(1): p. 127-36.
50. Grant, D.S., et al., *Two different laminin domains mediate the differentiation of human endothelial cells into capillary-like structures in vitro.* Cell, 1989. **58**(5): p. 933-43.
51. Basu, G.D., et al., *A novel role for cyclooxygenase-2 in regulating vascular channel formation by human breast cancer cells.* Breast Cancer Res, 2006. **8**(6): p. R69.
52. Scavelli, C., et al., *Vasculogenic mimicry by bone marrow macrophages in patients with multiple myeloma.* Oncogene, 2008. **27**(5): p. 663-74.

53. El Hallani, S., et al., *A new alternative mechanism in glioblastoma vascularization: tubular vasculogenic mimicry.* Brain, 2010. **133**(Pt 4): p. 973-82.
54. Bussolati, B., et al., *Endothelial cell differentiation of human breast tumour stem/progenitor cells.* J Cell Mol Med, 2009. **13**(2): p. 309-319.
55. Bruno, S., et al., *CD133+ renal progenitor cells contribute to tumor angiogenesis.* Am J Pathol, 2006. **169**(6): p. 2223-35.
56. Goldman, O., et al., *Endoderm Generates Endothelial Cells during Liver Development.* Stem Cell Reports, 2014. **3**(4): p. 556-65.

9 ACKNOWLEDGEMENTS

Sehr geehrter Herr Prof. Wagner, ich danke Ihnen dafür, dass sie mir die Chance zu dieser Arbeit gegeben haben, mich nicht aufgegeben haben und mich motiviert haben, es zu einem guten Ende zu bringen. Ich habe sehr viel bei Ihnen fürs Leben lernen dürfen, dafür ein herzliches: Vergelt's Gott!

Meinen Eltern möchte ich den größten Dank aussprechen! Ich hätte mir in all den Jahren des Großwerdens keine bessere Unterstützung vorstellen können als durch Euch. Danke, dass ihr immer an mich geglaubt habt und mich mit großem Selbstvertrauen und Selbstbewusstsein gestärkt ins Leben geschickt habt! Danke!!!

Hey große Lieblingsschwester, dir natürlich auch ein riesiges Dankeschön dafür, dass du immer ein offenes Ohr für mich hast, wenn ich es brauche, dafür, dass du immer für mich da bist, dafür, dass du bist wie du bist, und für all die lustigen Tage und Abende, die wir hatten und noch haben werden!

Den Hut zieh ich vor meinem Niclas. Du bist das Großartigste, was mir geschenkt werden konnte! Ich bin unendlich stolz auf deine Leistungen und werde es immer sein! Ich danke dir, dass du immer Geduld und Verständnis aufgebracht hast, wenn ich beruflich eingespannt und angespannt war oder an dieser Thesis schreiben wollte.

Ein riesiges Danke geht auch an Tini! Dafür, dass du immer beharrlich um meine Doktorfeier gekämpft und sie eingefordert hast, dass du mir beim Korrekturlesen unter die Arme gegriffen hast und natürlich nicht zuletzt auch für die vielen lustigen Befreiungsabende für Cuba!

Ein lautes „Ihr seid die besten!" geht raus an die üblichen Verdächtigen! Manu, Martin, Basti, Flo, Steffi, Steffi, Miri und Maria. Wo soll ich bei euch anfangen? Das würde ja kein Ende nehmen… Danke für all den Quatsch (letzter Wies'nsonntag, oldschool, Rock im Wald, etc.), den ihr euch immer einfallen lasst und den ihr

mitmacht, wenn er von uns kommt! Ohne euch wären die Tage höchstens halb so hell! DANKE!

Ein ganz herzliches Dankeschön geht an Ursula, Anna, Markus und Wolfgang. Ohne euch gäbe es den 3. Stock in Haus D vermutlich schon lange nicht mehr! Danke für all eure Unterstützung beim Bestellen, technischen Problemen und im Tierstall. Vor allem aber auch für all die gute Laune, die ihr ins Labor mitbringt und eure immer offenen Ohren für angeschlagene Doktorandenseelen!

Danke an Dr. Michael Günther für all die Vorarbeit an diesem Thema, deine Betreuung und all das, was ich von dir lernen durfte. Schade, dass du den Weg nicht ganz bis zum Ende mitgehen konntest. Ich wünsch dir, dass es die richtige Entscheidung war und du Glück und Erfolg mit deiner Familie und deiner Apotheke findest und gefunden hast!

Ein herzliches Danke geht an Martina für die lieben Aufmerksamkeiten, die du immer bescheiden und heimlich verteilt hast und damit so viel Freude und Lächeln verschenkt hast. Was wäre Fasching ohne dich gewesen? Und wer wollte je die Feuerzangenbowle missen? Danke!

Danke an Miriam für die tolle Unterstützung bei so vielen Versuchen und dass du dein Wissen über Zellkultur, Technik und so viele Methoden mit mir geteilt hast.

Danke an all die Mitdoktoranden, die ich kennenlernen durfte während meiner Zeit am Lehrstuhl. Ihr ward die besten Kollegen, die man sich wünschen kann! Ihr habt’s geschafft, dass ich gern zur Arbeit kam, selbst in Zeiten wenn’s versuchstechnisch nicht einladend war. Einen besonderen Platz in meinem Herz haben Edith (Frischluftbuddy), Thomas (der mit dem Dr. von Anfang an), David (Frequency), Arzu (Frequency), Christian (Frequency), Katarina (Q und Tierstall und überhaupt). Ihr seid die besten. Ich vermisse euch!

Der Schlusspunkt gehört natürlich der wichtigsten Person in meinem Leben: Mona, ich liebe dich! Ich möchte dir von Herzen dafür danken, dass ich bei dir so sein darf wie ich bin, dass du mich immer bei meinen Ideen und Vorhaben unterstützt und

mich bestärkst. Du gibst mir so viel, dass ich es gar nicht in Worte fassen kann und dafür einfach: DANKE!

An alle, die ich hier nicht namentlich erwähnt habe: Ich habe euch nicht vergessen, nur leider durften die Acknowlegements nicht länger werden als der wissenschaftliche Teil. Ich trage euch im Herzen und bin dankbar, dass ich euch kenne und dass mich so viele liebe und wertvolle Menschen begleiten!